Tectonics Journal
Vol 7, No 25, Spring 2023
doi 10.22077/jt.2024.6691.1162

University of Birjand

Analogue upright folds in the Sao Francisco Congo Craton deformed margin, Central African Fold Belt (CAFB). Inferences to the Western Gondwana tectonic evolution

Vincent Ngako[1], Emmanuel Njonfang[2]*, Julien Bernard[3], Jean Marcel Abate Essi[1-3], Yannah Mero[1], Augustin Patrice Moussango Ibohn[1], Sylvestre Ntomba[1], Yaya Fodoué[1], Zénon Itiga[4]

1. Institut de Recherches Géologiques et Minières (IRGM) / Ministère de la Recherche Scientifique et de l'Innovation (MINRESI), Cameroun.
2. Laboratoire de Géologie, Ecole Normale Supérieure, Université de Yaoundé I, B.P. 47, Yaoundé, Cameroun.
3. Bureau de Recherches Géologiques et Minières (BRGM), 3 avenue Claude Guillemin, BP 3600945060 Orléans Cedex 1, France.
4. Department of Earth Sciences, University of Douala, P'O. Box 24157 Douala, Cameroon.

Received: 2023/11/20
Accepted: 2024/08/12

Key points

1.) Analogue folds boundary High Strain Zones materialize parallel shortening of east-west foliation trends and the finite strain geometry of Western Gondwana belts

2.) High Strain Zones serve as channels for magma ascent and granitoids emplacement in the upper crust.

3.) The belts finite strain geometry is inferred to the serial collisions of three major plates whose margins were more or less intensely reworked.

Abstract

Analogue upright folds in the Sao Francisco Congo Craton (SFCC) northern margin overprint an early flat–lying to E–W–directed moderate dipping XY deformation plane outlined by an S_{1-2} foliation. They display steeply dipping high strain zones (HSZ) parallel to the axial planes of first to fourth–order analogue folds. The HSZ widths are scaled to the fold order: discrete crenulation boundary HSZ scaled to the third and fourth–order folds, thick crenulation boundary HSZ scaled to the first and second ones. The HSZ morphology varies with the structural levels: in the shallow and medium–crustal levels, disjunctive and gradational–type cleavages prevail, whereas discrete and zonal–type mylonitic cleavages are ubiquitous in deeper levels where they interact with the emplacement of granitoids. Z– and S–types crenulation showing boundaries cleavages or HSZ characterize analogue fold limbs, and M–type ones, analogue fold hinges. These structural markers enable to reconstruct the first and second–order fold profiles from the geometry of regional S_{1-2} foliation trends. The resulting finite strain pattern materializes D_{1-2} and D_3 interference at global–scale. Two main stress directions are inferred from XY planes and layer parallel

*Email: enjonfang@yahoo.fr
Tel: +237 675 28 33 71

shortening: 1) the N20°E direction correlates with roughly E–W foliation trends marking the earlier nappes stacking episodes upon the SFCC (orogeny 1: 680–620 Ma), and 2) the N120°E direction correlates with meridian–directed nappes stacking episodes upon the West African Craton and F_3 fold nappes overprints in CAFB (orogen 2: 600–580 Ma).

Index terms: High strain deformation zones (code 8012), Continental margins : convergent (code 8104), Folds and folding (code 8005), pluton emplacement (code 8035), Gravity anomalies and Earth structure (0920, 7205, 7240) (code 1219).

Keywords: Finite strain pattern, High Strain Zone, Neoproterozoic fold belts, Plates' collision, Orogens 1 and 2.

1. Introduction

The mapping and reconstruction of global–scale folds are among the major structural challenges for geologists working in old and deeply eroded belts. Indeed, except the case of refraction, the cleavages, schistosity, and foliation mark the XY planes high strain zones (HSZ) of the ellipsoid of deformation (Ramsay & Hubert, 1983) which is parallel to the axial planes of analogue folds. Their intersection angles with the folds profiles enable to characterize the fold hinges and the fold limbs, irrespective to fold order and scale. This rule is particularly reliable in high–temperatures deep metamorphic terrains where ductile deformation and low rheological contrasts occur.

Structural assessment of analogue folds geometry and interferences in the Central African Fold Belt (CAFB) is of particular interest for the tectonic interpretations in western Gondwana. In the occurrence, the very strong transposition of the early foliation parallel to N–S–directed analogue folds masks the early trend and evolution of the belt. This tectonic feature has led to the strong emphasizes on the E–W–directed converging models between the West African Craton (WAC) and the SFCC over many decades (Affaton et al., 1991; Castaing et al., 1994; Liégeois et al., 1994; Mvondo et al., 2023; Penaye et al., 2006; Tchakounté Numbem et al., 2017; Toteu et al., 1990, 1991, 2001, 2004; Trompette, 1994). Though plate's convergence models have also been considered in the more recent years between the Eastern Sahara Craton (ESC) and the SFCC (Abdelsalam et al., 2002; Ngako et al., 2008; Ngako & Njonfang, 2011, 2018), many geologists find it difficult to conciliate this model with the N–S finite trend direction of the CAFB strongly marked by N–S elongated granitoid massifs (Mvondo et al., 2023). This situation maintains controversy among the collisional models, mostly due to the lack of a very clear structural picture of the belt, and the existence of still uninvestigated or inaccessible regions. In the previous studies, we inferred the meridian–directed trends of the CAFB to a two–stage collision of three converging plates involving the SFCC, the ESC, and the WAC (Ngako et al., 2008; Ngako & Njonfang, 2011, 2018). Our model relies on the evidence of an indent–like finite strain pattern in the SFCC margin, and the indenter–like geometry of its ESC counterpart (Figure 1). Indeed, the SFCC indent shows E–W–directed F_2 synclines and anticlines in the Poli region situated at the indenter front that are progressively overturned southwards into recumbent en echelon folds and nappes. These folds are coeval with N50°E–directed shear zones, the so–called Buffle Noir Mayo Baleo (BNMB) and Balche (BSZ) shear zones and their synthetics, the so–called Gode–Gormaya (GGSZ) and Mayo Nolti (MNSZ) shear zones. These early shear zones and en echelon folds are overprinted by F_3 meridian en echelon upright folds coeval with the N70°E–directed Central Cameroon Shear zone (CCSZ), and the coeval synthetics of the Vallée des Roniers

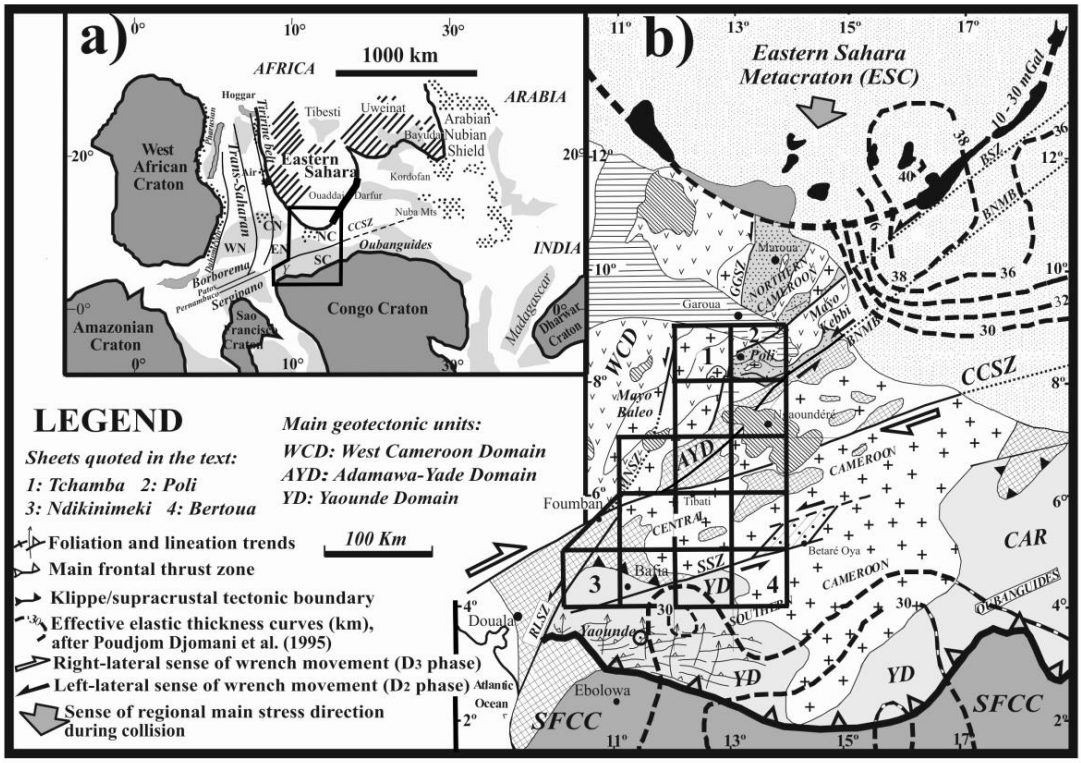

Quaternary sediments | Neogen volcanics | Mesozoic sediments (Benue trough) | Late syntectonic subalkaline granites | Lom syntectonic basin (syn-D_2 metasediments, conglomerates, volcanics ashes and lavas) | Western Cameroon Domain (Basic to intermediate calc-alkaline intrusion, 660-600 Ma) | a-Poli Group (Neoproterozoic front arc basin); b-Yaounde Group (Subduction-related back arc basin) | Massenya-Ouniangaa gravity highs (10-30mGal) | Adamawa-Yade and Nyong Paleoproterozoic units | Craton and inferred craton (metacraton). SFCC: Sao Francisco Congo Craton. CCSZ: Central Cameroon Shear Zone. CAR: Central African Republic

Figure 1. (a) Location of the CAFB study area in the Western Gondwana pre–drift map showing major cratons, metacratons, and High Strain Zones (modified after Küster and Liégeois, 2001). (b) Structural map of the belt in Cameroon showing its main geological domains (completed and modified after Toteu et al., 2004). The grid shows the areas covered by the Cameroon PRECASEM mapping project at 1/200.000.

(VRSZ), Demsa (DSZ) and Sanaga fault (SSZ) (Ngako et al., 2008). We infer those shear zones and folds systems to two plates convergent settings: the E–W setting, which led to orogen 1 opposes the ESC and the SFCC plates margin that collided prior to post–collision granulite nappes in eastern Nigeria at around 640 Ma (Ferré et al., 1998, 2002) and the N–S setting that led to orogen 2 opposes the SFCC and the WAC paleoplates, which collided at c.a. 630 Ma (Attoh et al., 1997; Black et al., 1979; Jahn et al., 2001).

In the present paper, we provide: 1) examples of the fractal geometry of first, second, and third–order F_3 folds analogues in the CAFB, using the intersection angles of boundary HSZ with the folds profiles at all scales, 2) the reconstruction of the belt early and late foliation trends from F_2 and F_3 folds overprints, and 3) the structural links between F_3 boundary HSZ, granitoids emplacements, and two collisional settings in Western Gondwana.

2. Geological and Tectonic Settings

Most authors consider the SFCC northern edge as a passive margin that collided, either with the WAC (Mvondo et al., 2023), the AYD (Tchakounte Numben et al., 2017; Toteu et al., 2022), or an intermediate basin and range domain with the WAC (Affaton et al., 1991; Trompette, 1994; Castaing et al., 1994). Geologic units involved in the collision are currently correlated to three main geotectonic settings or domains

(Toteu et al., 2004): the West Cameroon Domain (WCD), the Adamawa Yade Domain (AYD), and the Yaoundé Domain (YD) (Figure 1).

The WCD is a volcanic arc environment, which presently shows Neoproterozoic medium– to high–grade schists and gneisses derived from tholeiitic basalts and calc–alkaline rhyolites (Ngako, 1986; Njel, 1986) dated at c.a. 800 Ma (Toteu, 1990); pre–, syn–, to late–tectonic calk–alkaline granitoids including diorites, granodiorites, and granites emplaced between 660 and 580 Ma (Toteu et al., 1987, 2001). New geochronological data obtained during the PRECASEM mapping project (https://fr-sigm-online.hub.arcgis.com) in the south and west of this domain have revealed the presence of probable SFCC Paleoproterozoic recycled pieces in those Neoproterozoic assemblages. Post–tectonic rocks include alkaline granitoids (granites and syenites), mafic and felsic dykes, as well as sedimentary and volcanic rocks of the Mangbai–type series considered as probable Pan–African molasses (Bea et al., 1990 ; Montes–Lauar et al., 1997).

The AYD is considered as a block detachment of the SFCC margin following back–arc extension, magmatism, and deposition of supra–crustal material in the YD (Ngako et al., 2008; Ngako & Njonfang, 2011) or marking a pre–tectonic extension leading to separated plates (Tchakounté Numbem et al., 2017; Toteu et al., 2006, 2022). It shows large–scale pieces of Paleoproterozoic sedimentary and intrusive rocks metamorphosed in the granulite facies at 2.1 Ga, and reworked during the Pan–African tectonic evolution (Tchakounté Numbem et al., 2017; Toteu et al., 2001). This domain includes widespread syn– to late–tectonic granitoids mainly of transitional composition or crustal–derived origin (Ganwa, 2005; Soba et al., 1991; Tchakounté, 1999; Toteu et al., 1994, 2001).

The YD is diversely interpreted, either as epicontinental, intracratonic or passive marginal setting (Nzenti et al., 1988), a back–arc basin (Ngako et al., 2008; Ngako and Njonfang, 2011) or intra–oceanic domain separating convergent plates (Tchakounté Numbem et al., 2017; Toteu et al., 2001). It evolved as a huge nappe of metasedimentary units including large sheets of pre– to syn–tectonic plutonic rocks, presently represented by low– to high–grade garnet bearing schists, gneisses, and orthogneisses metamorphosed under medium– to high–grade granulite facies (Nedelec et al., 1986; Nzenti et al., 1988). Pressure (P)–Temperature (T) conditions yield T = 750–800°C and P= 10–12 kbars (Barbey et al. 1990; Mvondo et al., 2003). Plutonic rocks mostly include mafic to intermediate rocks, best represented by the Yaoundé pyriclasites and the serpentinized nickel–chromite bearing rocks, gabbros, diorites, and mafic dykes in the Lomié and Boumyebel regions (Seme Mouangue, 1998; Yongue Fouateu, 1995; Yonta Ngoune et al., 2010). The Boumyebel and others MORB–like rocks found therein are presently interpreted as oceanic floor remnants obducted during convergence and collision of the SFCC with AYD (Fuh Calistus et al., 2021; Mukete Kundu et al., 2022; Nkoumbou et al., 2006; Toteu et al., 2022; Yonta Ngoune et al., 2010). Late– to post–tectonic granitoids are very scarse in this domain.

The tectonic evolution of CAFB includes an early S_1 foliation transposed into S_{1-2} and refolded by E–W–directed F_2 synclines and anticlines progressively overturned southwards into recumbent folds and nappes overriding the SFCC undeformed margin. The most representative feature of the nappe is an early low–plunging L_{1-2} lineation directed N–S and a flat–lying S_{1-2} foliation refolded by F_3 upright folds (Figure 2 and 6). The L_{1-2} lineation map (Figure 3) characterizes two different kinematic

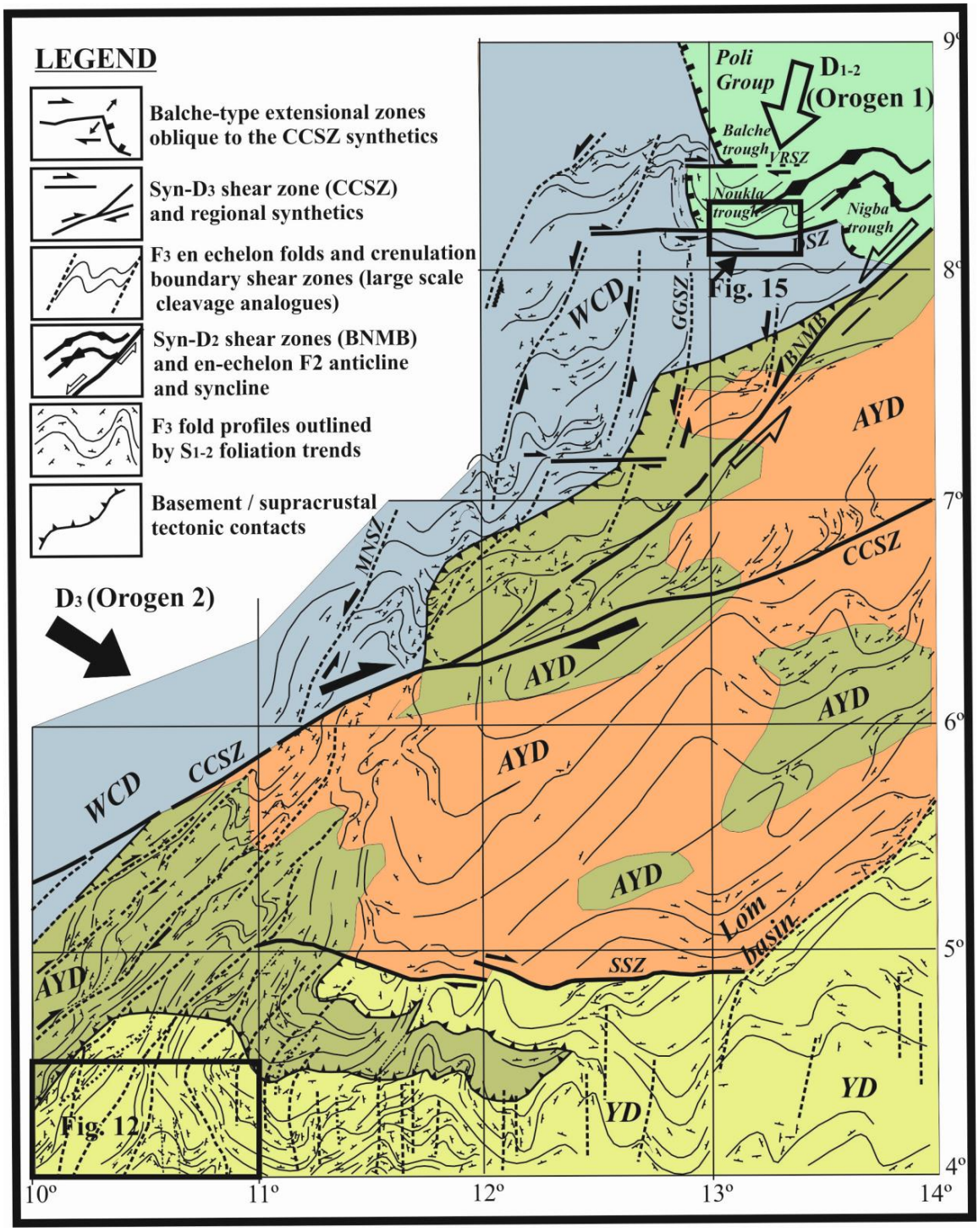

Figure 2. Structural map of the study area (S_{1-2} foliation measurements in the late–tectonic granitoids were made on refractory minerals or partially melted rocks). The WCD, AYD and YD domains are from Toteu et al. (2004).

directions in the refolded nappe. In the north of the SFCC and up to the BNMB shear zone, lineations are directed N–S to NNE–SSW. Beyond the BNMB shear zone toward the west, they are directed E–W to NW–SE. In the first group, the lineations materialize the nappe displacements onto the SFCC. Their interaction with dextral shear movements in the CCSZ and synthetics of the SSZ shows progressive clockwise rotation marked by S–type trends. According to the experimental and

natural indentation models (Cobbold & Davy, Davy & Cobbold, 1988; Taponnier et al., 1986), the second group of lineations materializes the westward displacements of lateral escape nappes in the SFCC indent during indentation by the ESC prong (Ngako et al., 2008; Ngako & Njonfang, 2011). Very likely, the original directions of these lineations were slightly modified by F_3 folds and right–lateral rotation of the region during dextral shear movements in the CCSZ. The occurrence of northeast verging nappes in Eastern Nigeria (Ferré et al., 1998, 2002) and westward verging nappes in WCD suggests the existence of intra–nappes thrust zones in CAFB.

The mean–direction of foliation trends is statistically defined from the correlation of outcrop S_{1-2} measurements. The inferred finite strain pattern shows large–scale F_3 meridian folds resulting from the interference of D_3 and D_{1-2} deformation phases. S_{1-2} crenulation boundary high strain zones (HSZ) at the map–scale are crenulation boundary cleavages analogues. HSZ boundaries of the Z– and S–types crenulations materialize the western and eastern limbs of the first–order folds, while HSZ boundaries of M–type crenulations materialize their hinges in Poli and YD, respectively. The AYD includes intra–nappe basement pieces incorporated in the WCD and YD supra–crustal units boundary and intensely reworked during the Pan–African tectonic evolution.

3. F_3 Folds analogues in CAFB

3.1. First–Order Folds

The hinges and limbs of first–order F_3 folds in CAFB are inferred from the Z–, S–, and M–type second–order crenulation and boundary HSZ (Figure 2). Indeed, in analogy with the third or fourth–order crenulations, second–order folds show repetitive or rhythmic profiles and boundary HSZ materializing the XY plane of the ellipsoid of deformation parallel to their axial plane. Practically, M–type second–order fold with high strain boundaries (HSB) materialize the hinges of F_3 first–order fold, whereas Z– and S–type second–order fold with HSB materialize the limbs (Figure 4). After Borradaile et al. (1982), small–scale crenulation boundary cleavages include various morphologies. They are defined as gradational and discrete cleavages, continuous cleavages (e.g. schistosity), differentiated or zonal cleavages (e.g. foliation), and disjunctive crack–like boundary cleavages (e.g. fractures and joints) whose direction is parallel to the folds axial planes (Figure 4). The exception to this rule is when cleavages refraction occurs at layers interfaces showing strong rheological or competence differences (Figure 4b). The axial plane HSZ types vary with the Pressure–Temperature conditions in the belt successive structural levels. Brittle and semi–brittle HSZ (e.g. fractures, joints, schistosity, and cleavages refraction) mostly occur in the shallow–crustal levels, whereas semi–ductile and ductile ones (e.g. foliation) occur in moderate and deep–crustal levels.

The mean–directions of the lineation trends are statistically defined from outcrops measurements throughout the CAFB study area. They show a bulk N–S direction, except to the north of the CCSZ where NE–SW and NW–SE directions correlate with the extensional direction oblique to the BNMB shear zone and to westward nappes displacements. S–type lineation trends in the AYD and YD mark right–lateral rotation parallel to the cross–cutting shear zones and synthetics (CCSZ and SSZ) during D_3.

Z– and S–types crenulations materialize the western and the eastern limbs of analogue folds, whereas M–types crenulations materialize their hinges. Note that the folds limbs and folds hinges of different folds orders share similar angular relationships with crenulation boundary cleavages and HSZ at different scales, except in the cases of

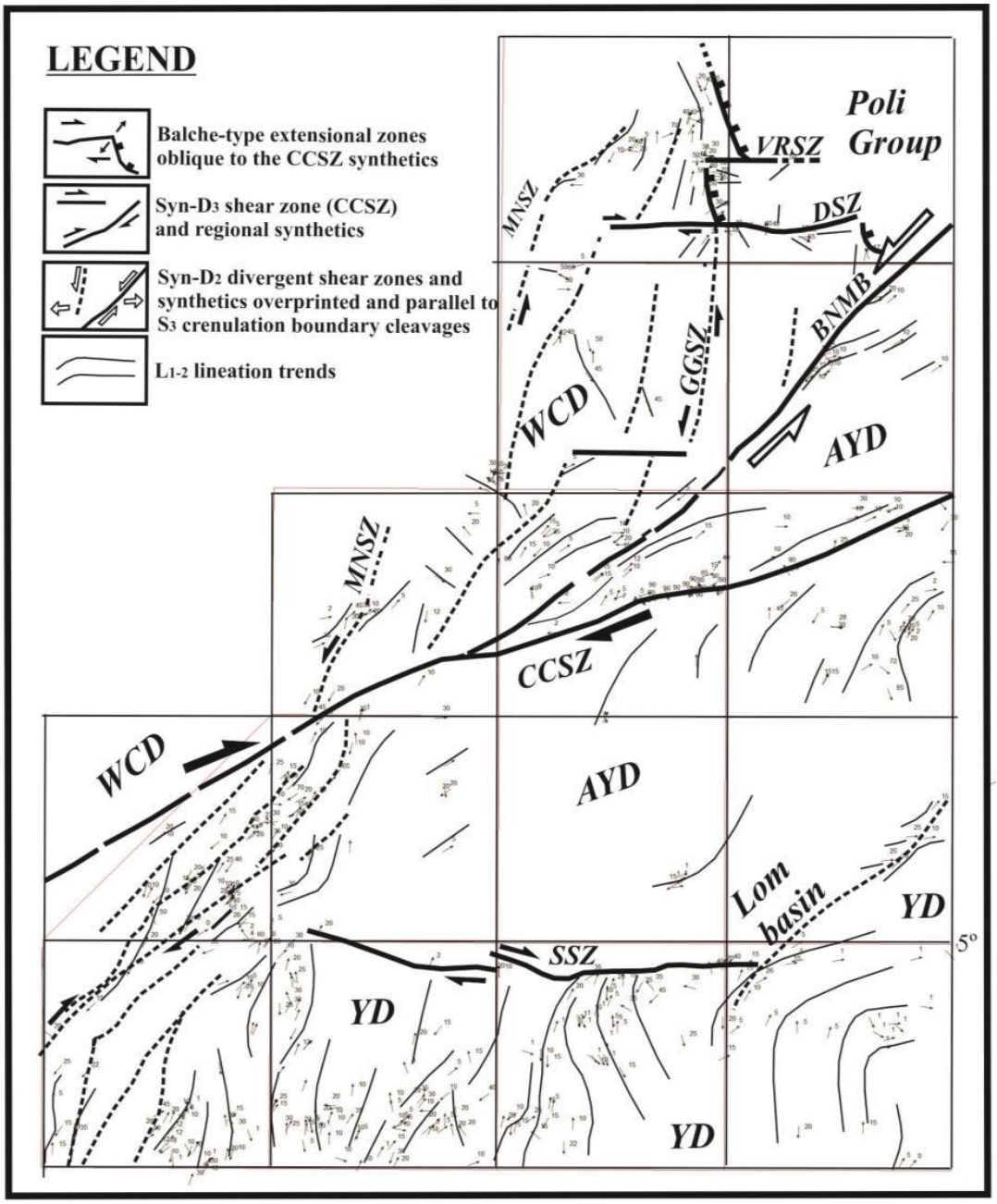

Figure 3. L_{1-2} mineral lineation trends map in the study area.

cleavages refraction at the layers interfaces marking strong competence differences. As well, the crenulation boundary cleavages intervals and frequency also vary with layer's rheology (or competence). In this Figure, rheology is weak in layer A, very strong in layer B, very weak in layer C, and moderate in layer D. Outcrops 1 and 2 show Z–type crenulations materializing the partial view of first–order fold left limb; outcrops 3 and 4 show S–type crenulations materializing the partial view of first–order fold right limb; outcrops 5 and 6 show M–type crenulations materializing the partial view of the first–order fold hinge.

In the SFCC deformed margin, F_3 folds result from inhomogeneous layer parallel shortening of S_{1-2} foliation as an accommodation of planar anisotropy and rheological differentiation in the lithologic layers piles. In the Poli lower–grade schists, continuous cleavages–types and chevron–types gradational crenulations are

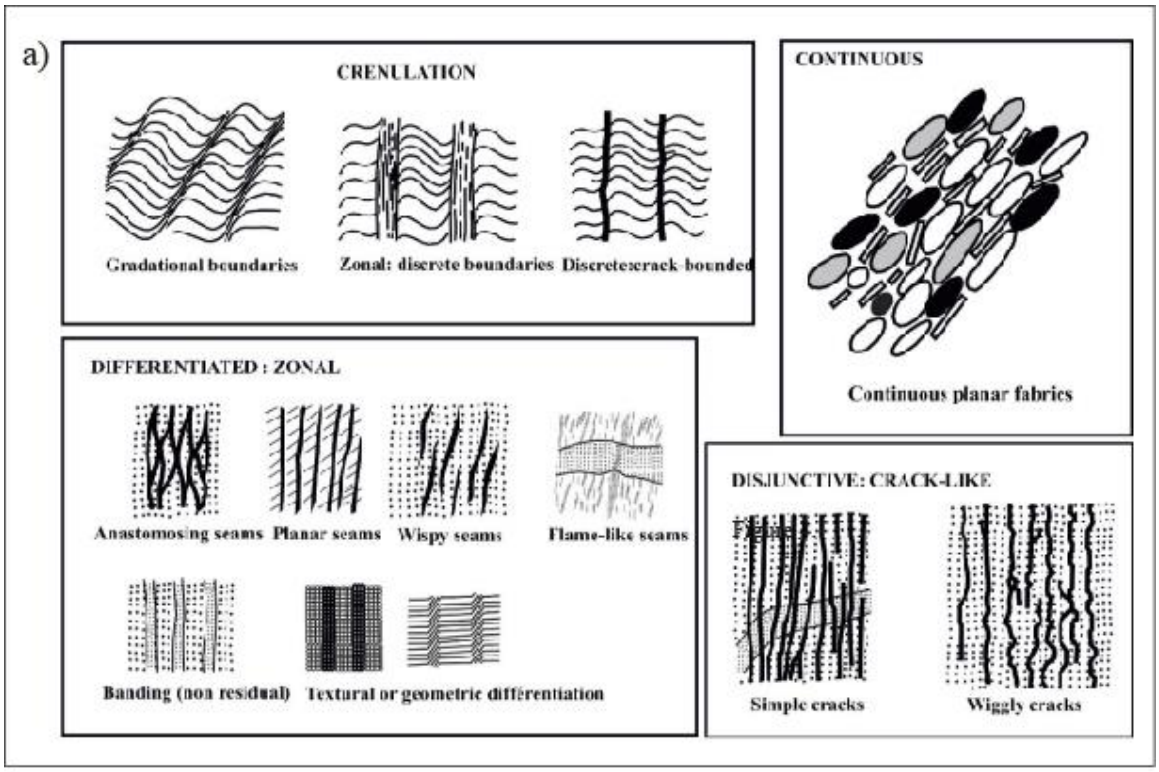

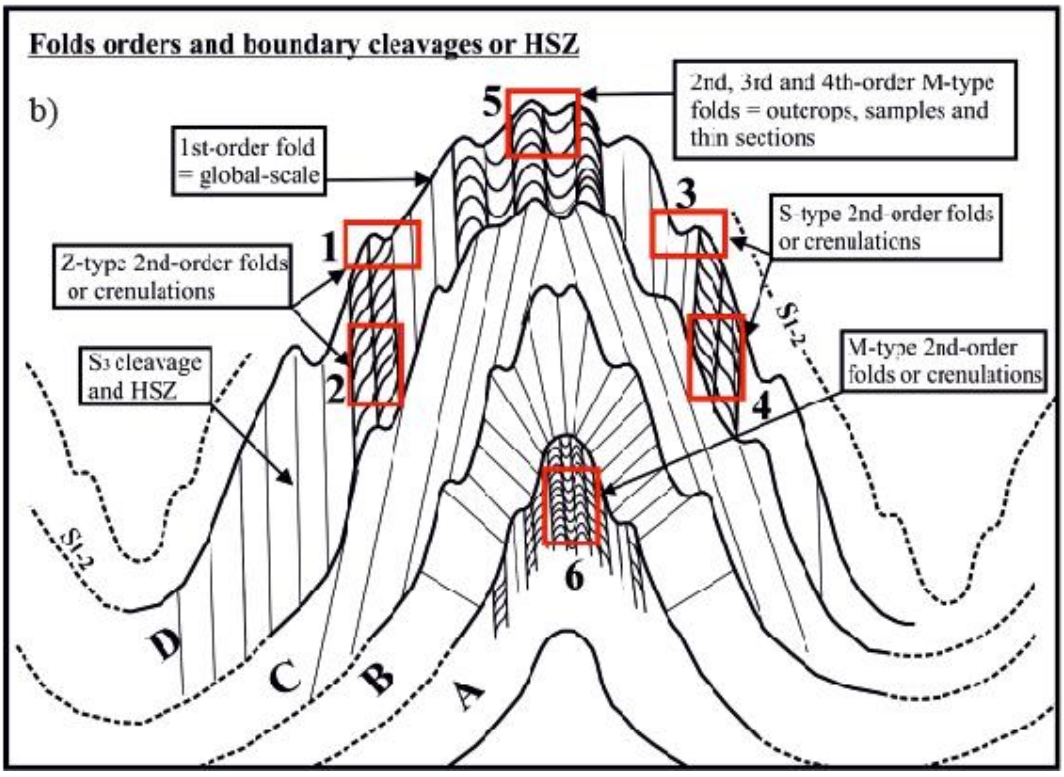

Figure 4. (a) Morphological types of crenulation boundary cleavages in deformed rocks (after Borradaile et al., 1982). Cleavages represent highly strain zones (HSZ) while microlithons represent weakly (WSZ) and mildly (MSZ) strain zones showing crenulations (rhythmic folds), eventually. (b) Idealized model of folds and crenulation boundary HSZ (cleavages) in analogue folds.

the most frequent (Figures 5a and 5b). In deep metamorphic high–grade gneisses, layer parallel shortening generates weakly (WSZ), mildly (MSZ), and highly (HSZ) strain zones that result in the development of crenulations with boundary cleavages and the more or less transposition of S_{1-2} foliation into parallelism with the HSZ (Figures 5c, 7a and 7c, and 8). WSZ and MSZ are referred to as microlithons, mesolithons, and megalithons that correspond to the fourth, third–second and first–order folds, respectively. Megalithons and mesolithons represent map and outcrop–scales microlithons analogues. The geometry of the related first, second, third, and fourth–order folds is fractal since the repetitive hinges and limbs analogues exhibit similar Z–, S–, and M–type crenulation boundary HSZ or cleavages (Figures 2, 4b, and 5). The progressive layer parallel shortening results in the increasing amplitudes of the crenulations and the progressive mylonitization of the lithons and microlithons, as well as the progressive widening of the mylonitic zone (Figures 5a and 7). In the final and the most advanced stages, the strong transposition of S_{1-2} foliation into parallelism with S_3 cleavages results in the development of regional HSZ (Figures 7a and 7b) mapped and reported so far as the BNMB synthetic shear zones (Bella Nke et al., 2018; Fozing et al., 2021; Kwékam et al., 2020; Ngako et al. 2008; Ngako & Njonfang, 2011; Nguiessi

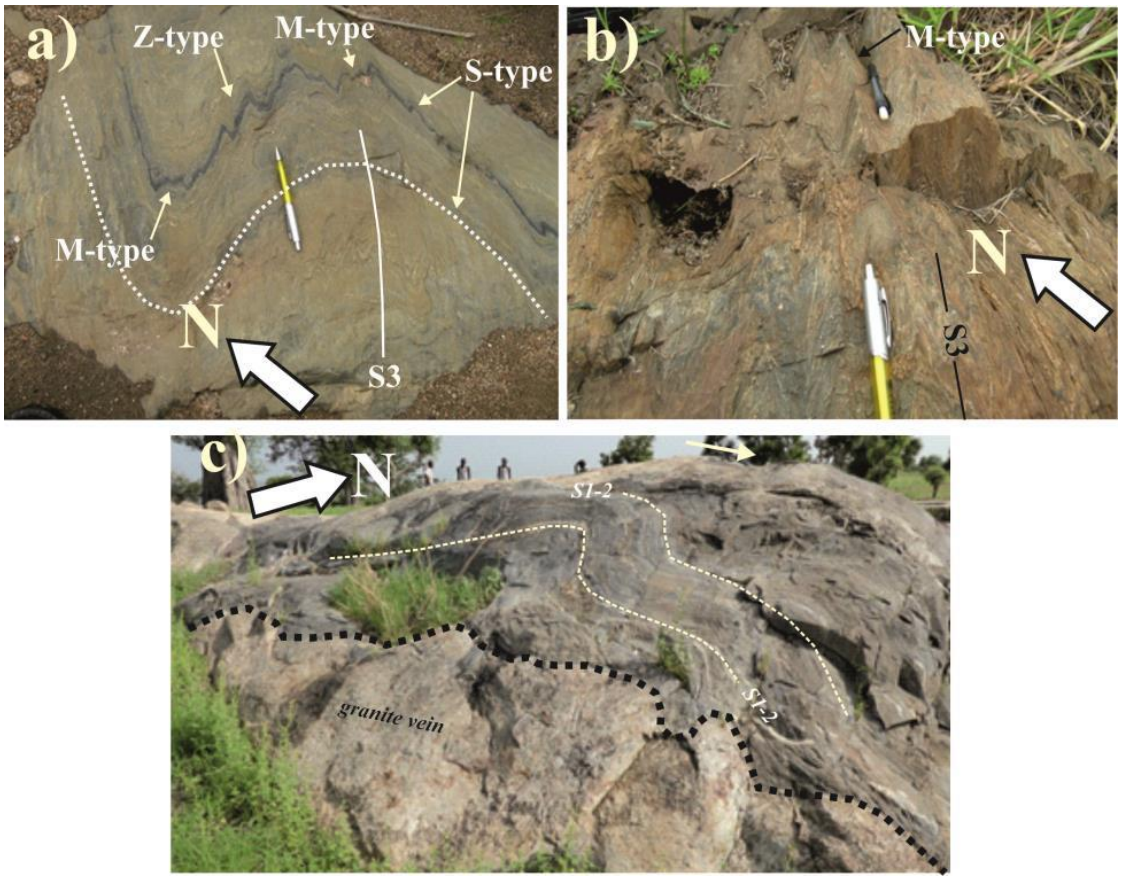

Figure 5. Structural features of meso and megalithons. Lithons represent WSZ and MSZ characterized by F_3 second and third–order analogue folds of various wavelenghts and amplitudes (crenulations).

Tchankam et al., 1997; Njiki Chatué et al., 2020).

Poli low–grade schists: (a) Right limb partial view of F_3 second–order fold showing a third–order S–type fold (or crenulation). Note that the limbs and hinges of the latter exhibit fourth–order Z–, S–, and M–type analogue folds or crenulations, respectively. Also note that S–type analogue folds correlate with the folds right limbs irrespective to orders. The rock schistosity or cleavage is of continuous–type parallel to the folds axial plane and intersects the fold profile at high–angles in its hinge zone and at low–angles in its limbs. (b) M–type crenulations with gradational boundary cleavages marking the hinge of a second–order F_3 fold; the fold axes plunge gently to NE at 20° (pencil). (c) ***Tchamba high–grade gneisses:*** WSZ showing low–amplitude second–order F_3 fold (anticline) plunging gently to the north and a syn–D_3 granitoid vein parallel to S_{1-2} foliation trend (TCH_6134).

However, according to the above principle, Z–, S–, and M–type S_{1-2} foliation trends exhibiting boundary HSZ in the study area (Figure 2) enable to determine the limbs and hinges of the first–order F_3 fold in the CAFB in Cameroon. In the WCD situated to the north of the CCSZ, S_{1-2} foliation trends show Z–type crenulation with HSB, materializing the western limb of the F_3 first–order fold and its transition towards the fold hinge in the Poli region (Figure 2). In the southwest of the AYD situated to the south of the CCSZ, S_{1-2} foliation trends show S–type crenulations with HSB that clearly materialize the western limb of the first–order fold analogue in the Yaoundé domain (Figure 2). Therefore, the juxtaposition of Z– and S–type crenulations in one and either side of the CCSZ in these two regions results from the right–lateral relative displacement of the opposite limbs of the F_3 first–order fold during shear evolution in the late–stages of the folding event. The WCD and the YD exhibit partial views of the western and eastern limbs of the first–order F_3 fold, which were dextrally shifted along the CCSZ and juxtaposed during the late–D_3 evolution (Figure 9). The reconstruction of the F_3 fold profile prior to this tectonic event is attempted using the correlations of S–type foliation trends in one and either side of the CCSZ. The general S_{1-2} foliation trends inferred from these correlations enable to outline the profiles of first–order F_3 folds whose axial plane is directed N30°E, parallel to the HSZ (Figure 6a). From the comparison of the present day and pre–CCSZ regional strain patterns (Figures 2 and 9), it appears that the western and eastern limbs of F_3 first–order folds were dextrally shifted from position "A" to position "B" over about 330 km along the CCSZ during the late–D_3 stages (Figure 9). The layers parallel shortening direction inferred to the tectonic stress direction during D_3 is approximately N120°E.

3.2. Second and Third–Order Folds

The structural map of Ndikinimeki region exhibits second–order meridian–directed rhythmic F_3 folds showing N–S boundary HSZ (Figures 1, 2 and 10a). HSZ are parallel to the axial planes of analogue F_3 second–order folds. At the regional and global–scales, this system corresponds to the CCSZ en echelon folds (Figure 2). The evolution of both structures correlates with an N120°E shortening direction. Parallel shortening of the S_{1-2} foliation generated F_3 meridian upright folds whose evolution ended with dextral shear displacements parallel to the CCSZ. At the outcrops–scale, the variations of F_3 folds directions result from the relative rotation of respective fold axes into parallelism with the CCSZ and synthetics near to their contact.

The finite strain pattern resulting from D_{1-2}

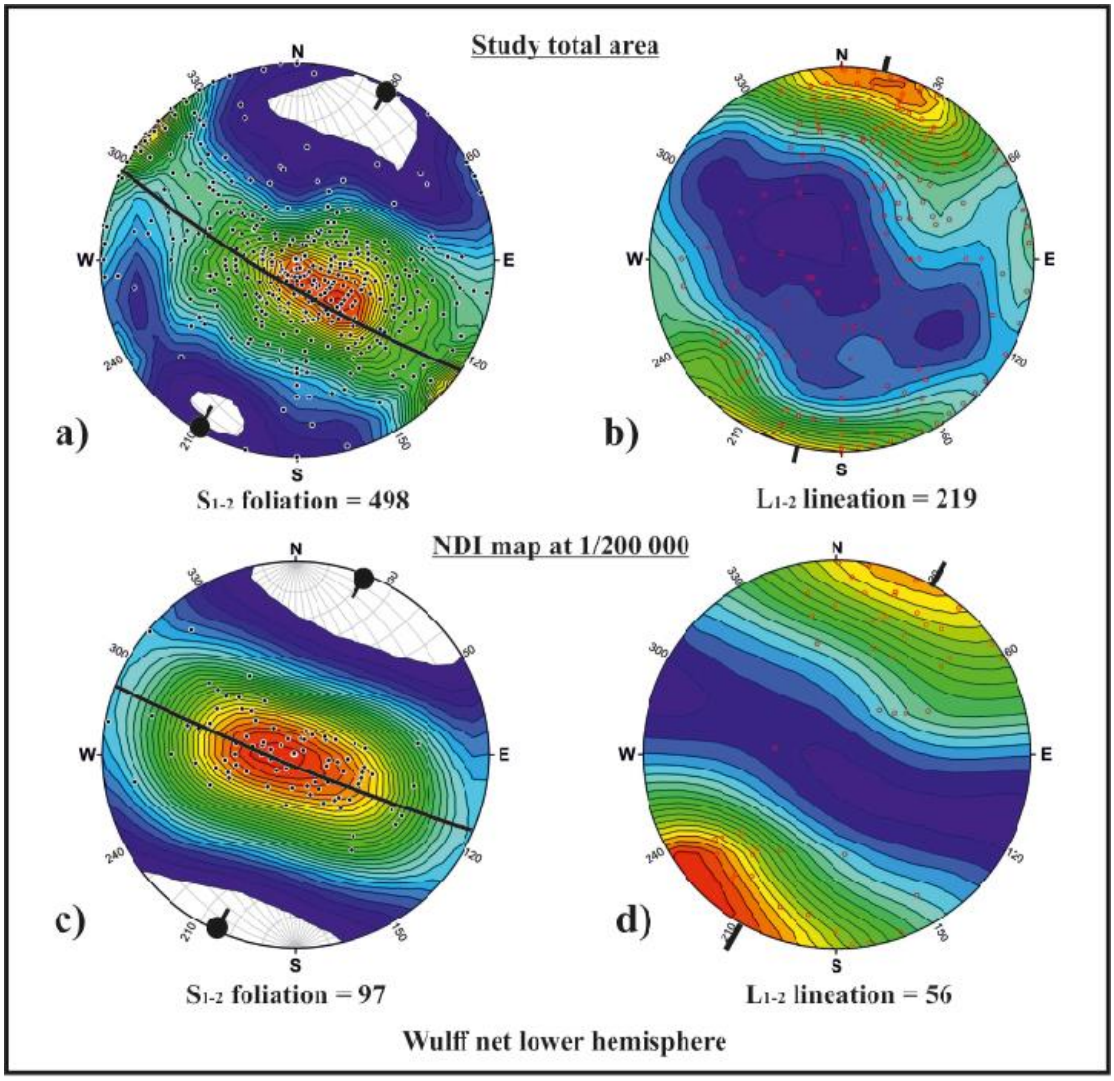

Figure 6. Foliation and lineation plots in the study area and in the southern NDIKINEMIKI sheet at 1/200 000 (Wulff net lower hemisphere). (a) and (c) S_{1-2} foliation poles (black dots in white circle) are distributed along a great circle whose pole determines the F_3 folds axes (thick circle). Most foliations gently dip southward and the direction of great circle shows the foliation mean original trend. (b) and (d) L_{1-2} mineral lineation plots show high density measurements of low to horizontal plunges parallel to F_3 fold axes, while scattered plots represent folded and more or less transposed lineations parallel to F_3 fold limbs and HSZ.

and D_3 interference shows a large–scale alternation of MSZ and HSZ. It marks a multistage tectonic evolution including an early S_{1-2} foliation originally directed E–W, inferred to N–S shortening, and F_3 meridian overprinting folds with boundary cleavages or HSZ inferred to layers parallel shortening (Figures 7a and 7b, and 10a). MSZ materialize megalithons and show successive F_3 second–order anticlines and synclines whose boundary HSZ may show steep to moderate dips. These folds exhibit either S–, Z– or M–types profiles, which characterize pure shear markers inferred to the D_3 phase of deformation (Figure 4b). F_3 folds axes in both domains often show low plunges, which suggest that the folded S_{1-2} metamorphic planes materialize an originally flat–lying to moderately dipping nappe (Figure 6c). Steep plunging F_3 folds axes are casual and likely occur only where they interfere with steep dipping S_{1-2}

foliation marking the reverse limbs of F_2 recline folds while low to moderate F_3 folds axial plunges occur where F_3 folds interfere with low to moderate dipping F_2 normal limbs. Boundary HSZ materialize meridian–directed mylonitic cleavages analogues as well as the XY main deformation plane of the ellipsoid of deformation. The Ndikinimeki finite– strain pattern in whole is analogue to the Borradaile small–scale crenulations and discrete–types boundary cleavages (Figure 4). It shows that the AYD is a syn–D_2 nappe inclusion or klippes in the YD and that both domains exhibit similar D_{1-2} and D_3 ductile deformation phases materialized by S_{1-2} foliation and F_3 first and second–order folds overprints (Figures 2 and 10a). No rigid block or map–scale intra–nappe boudins inferred to the AYD is allegeable. In the contrary, S_{1-2} foliation trends in this domain are parallel to the equivalent XY planes in the YD. F_3 folds geometry and S_{1-2} foliation trends in both domains exhibit similar complete transposition of the oldest Paleoproterozoic structures parallel to the Pan–African ones during D_{1-2} and D_3 ductile deformation phases (Figures 2 and 10a).

The development of HSZ in the study area results in the formation of more or less thickened boundary mylonites. Further to the north (Figure 7), discrete– and zonal–type mylonitic cleavages exist. Discrete–type outlines thin millimeter HSZ, and zonal–type shows thicker HSZ up to 4–5 centimeters and meters. Two main types of zonal cleavages are distinguished: the granitic– and the mylonitic–types (Figures 7 and 11).

The granitic–types correlate with HSZ and clearly suggest that they served as channels or conduits to anatectic melts migration and ascent to the upper crust. The increasing volumes of granite melts in the crenulation boundary cleavages resulted in the emplacement of granitoid veins and massifs at various scales and structural levels (Figure 11).

The mylonitic–types show progressive stages of mylonitization of mesolithons. In the more evolved stages, they are almost completely mylonitized and show only isolated remnants in the HSZ (Figures 7 and 10b). However, F_3 fold hinges and limbs can be easily identified from S_{1-2} and S_3 intersections angles, enabling the reconstruction of the second–order fold profiles. The geometry of the F_3 fold profile outlined by S_{1-2} foliation trends in the mesolithons remnants enables to reconstruct a decametric–size second–order F_3 fold in the Tchamba HSZ (Figure 10b). The interaction of M–, S–, and Z–type fold patterns in mesolithons characterizes coaxial evolution of the D_3 deformation phase.

Note that the mylonitization of mesolithons is progressive and increases from the stage of discrete boundary cleavages to the advanced stages of zonal boundary HSZ where only lense–type remnants of the mesolithons (marker) are preserved. The S_{1-2} foliation is directed N70°E and boundary HSZ are vertical at N160°E (TCH_6084 outcrop YZ horizontal section). Marker length is 14 cm.

3.3. Fold Hinge Interference with Synthetic Shear Zones

Unlike the western regions of the belt, where a dense network of thick HSZ occurs, analogue strain zones in the Poli and Yaoundé domains are scarce and discrete (Figure 2). This structural contrast materializes a strain variation and strain gradient across the F_3 folds profiles at all scales. HSZ in the fold limbs alternate with narrow mesolithons, whereas WSZ and MSZ materializing equivalent mesolithons in the fold hinges are wider. F_3 megafold hinges in both domains are crosscut by the CCSZ synthetic shear zones, the so–called VRSZ, BSZ, and SSZ, respectively (Figure 2). In the Poli region, the DSZ and the VRSZ interacted with down–slip

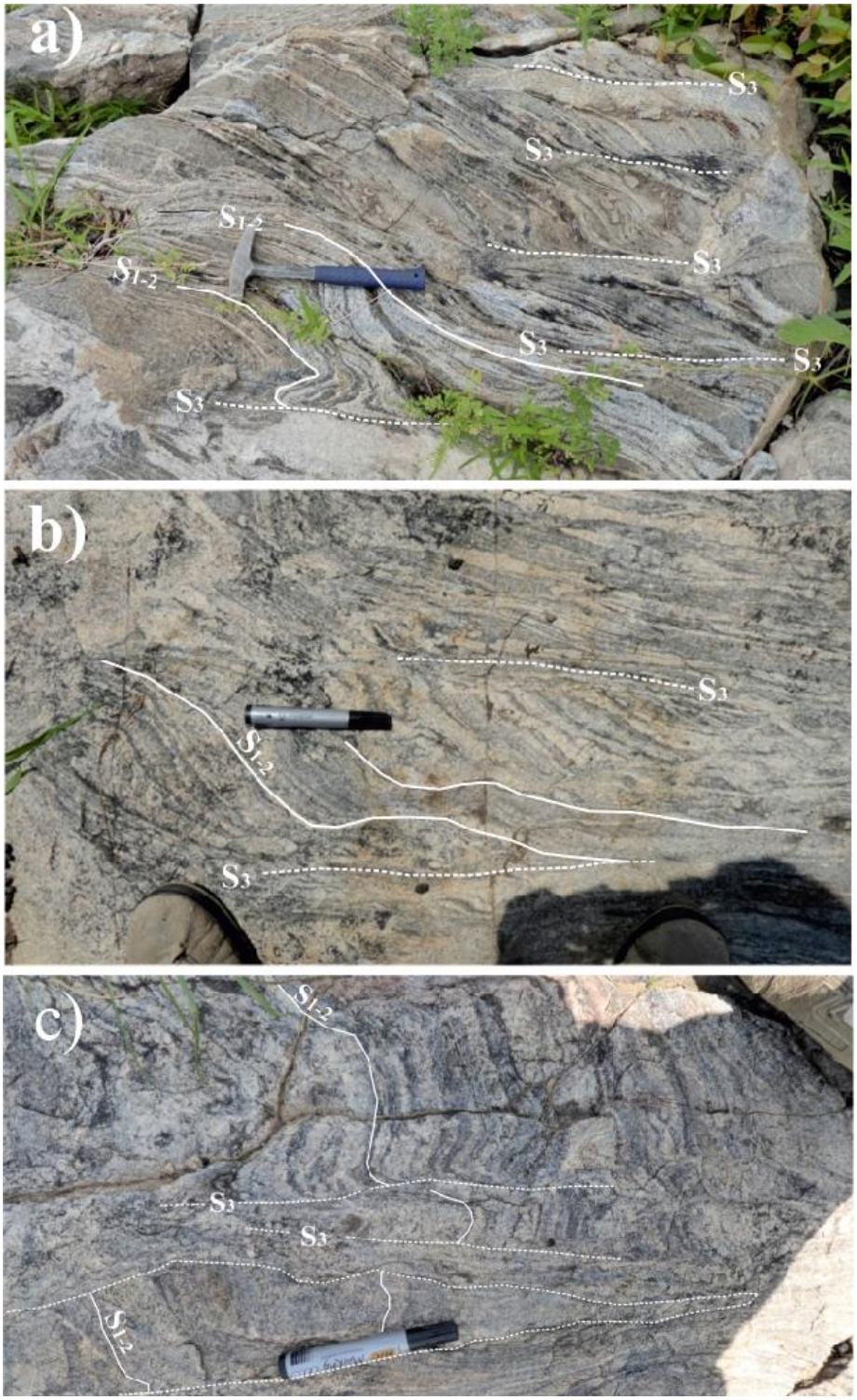

Figure 7. Structural features of HSZ. Note that mylonitization is progressive in the mesolithons boundary HSZ parallel to S_3 cleavages (Tchamba migmatites, sheet 1, Figure 1). (a) Early stages of mylonitization following discrete Z–type crenulation boundary cleavages locally intruded by granitic veins across the left limb of F_3 second–order fold (TCH_6079; S1–2 foliation is directed N50°E and Hanmer length is 30 cm. (b) Advanced stages of mylonitization in zonal Z–type crenulation boundary cleavages across the left limb of F_3 second–order fold. Remnants of mesolithons (black marker) result from incomplete mylonitization and transposition of $S_{1–2}$ foliation into parallelism with S_3 at this stage. (TCH_6084; $S_{1–2}$ foliation is directed N160°E and the black marker length is 14 cm). (c) F_3 second–order fold hinge showing axial plane discrete– and zonal M–type crenulation boundary HSZ parallel to S_3 cleavages (Tchamba orthogneisses: sheet 1, Figure 1).

displacements of the Poli Group along the Gode–Gormaya meridian HSZ (Figures 2 and 9). This kinematic evolution resulted in the juxtaposition of the Poli low to moderate–grade metamorphic schists (upper crustal levels) with the high–grade granulitic gneisses (deep–crustal levels). Likely, the GGSZ and DSZ boundary faults separating these metamorphic domains were further reactivated during the regional isostatic evolution generating the Balché, Noukla, Nigba, and Mangbai–type trenches (Figure 2). This evolution started with volcanic activity in the Balche trough at

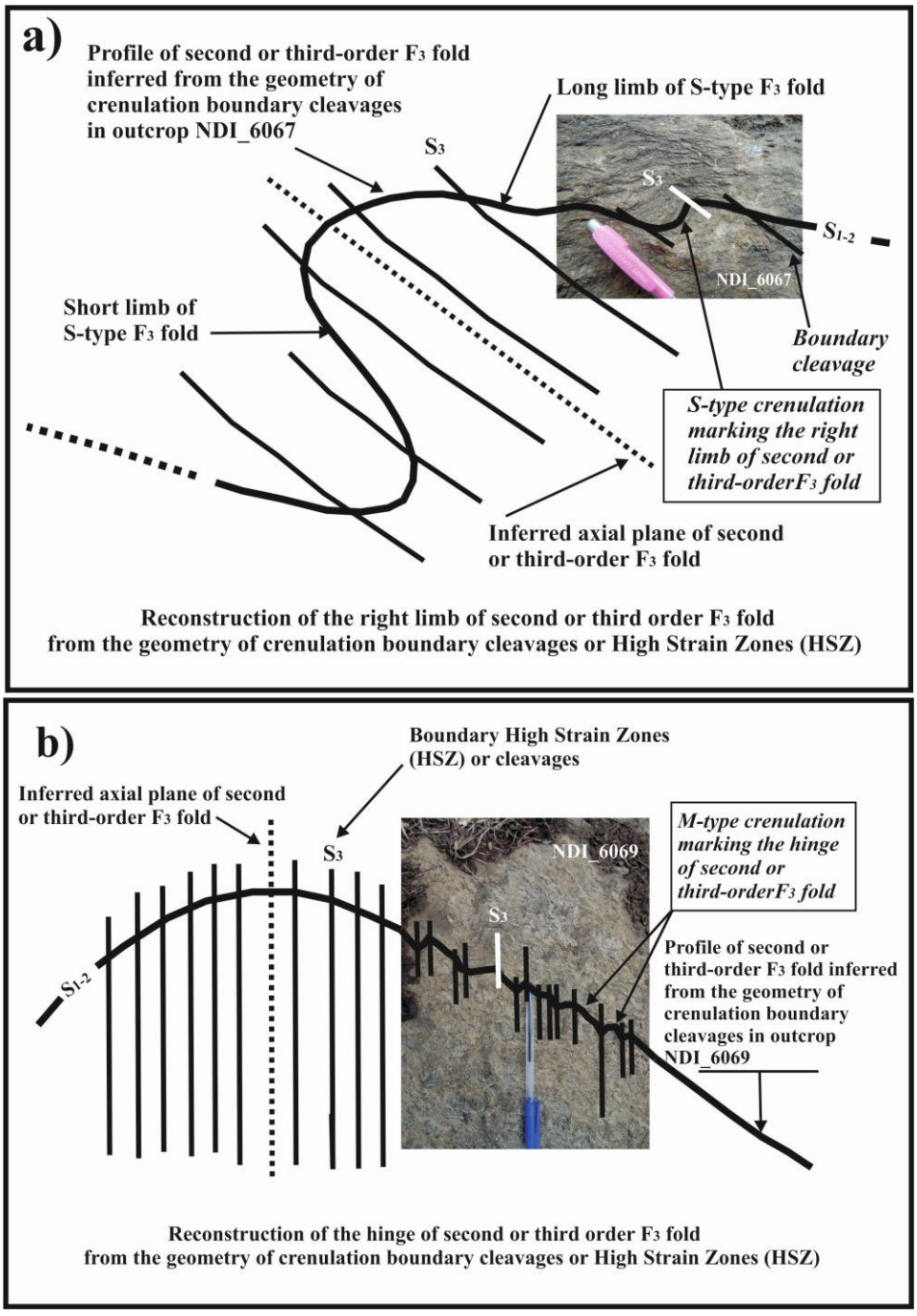

Figure 8. Second or third–order F_3 fold profiles reconstructed from outcrops partial views showing crenulation boundary cleavages in the Ndikinimeki orthogneisses (sheet 3, Figure 1). (a) Outcrop NDI_6067: gradational S–type crenulation boundary cleavages marking the right limb of F_3 second–order fold. (b) Outcrop NDI_6069: gradational boundary cleavages marking the hinge of F_3 M–type second–order fold.

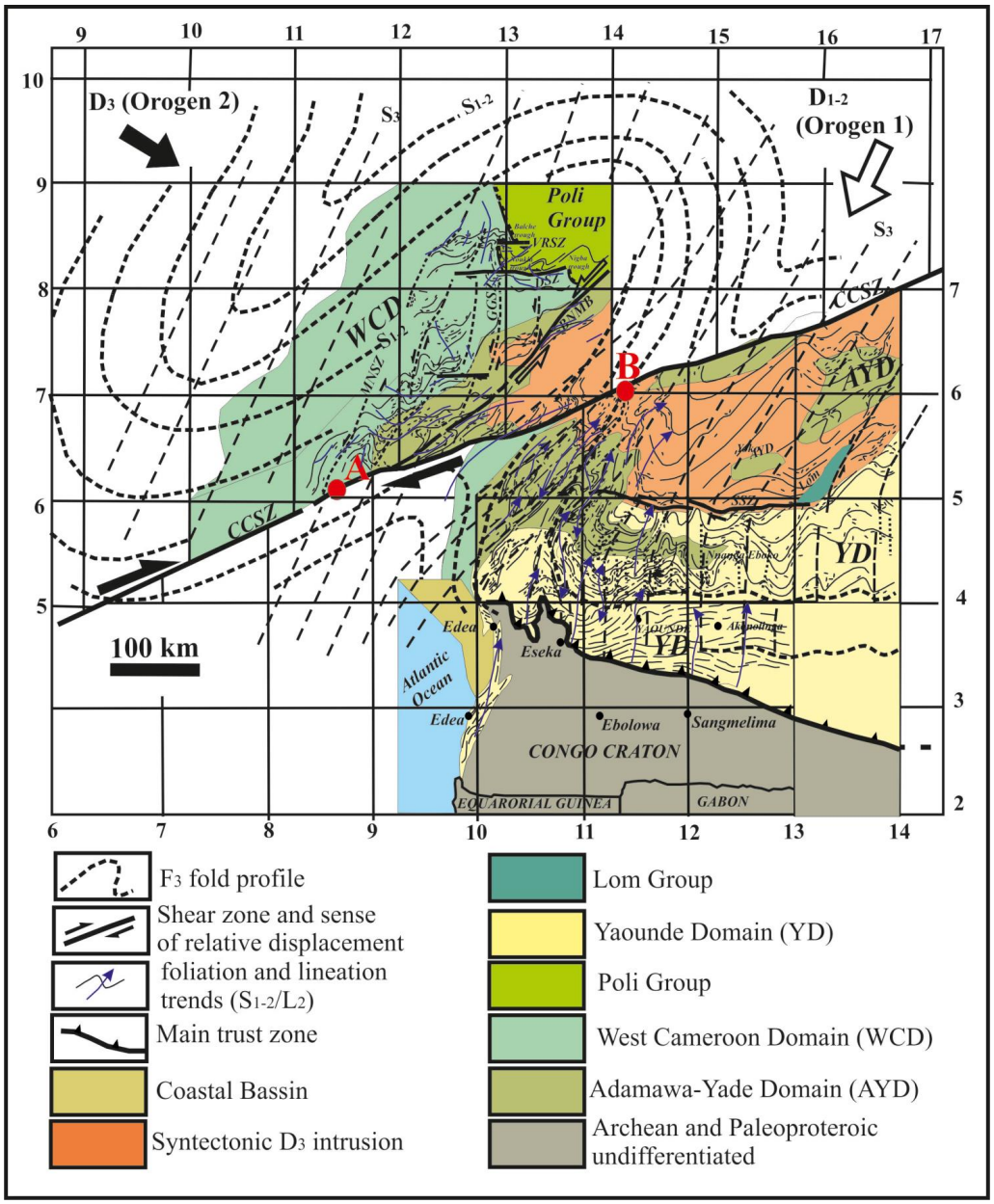

Figure 9. First–order F_3 folds reconstructed from the map–scale Z–, S–, and M–types $S_{1–2}$ foliation trends in the SFCC deformed margin ($S_{1–2}$ foliation trends in the Congo Craton northern margin are from Jégouzo, 1984).

c.a. 580±20 Ma (Rb–Sr isochron age by Montes–Lauer et al., 1997).

Z–type foliation boundary HSZ in WCD characterize the fold western limb; S–type foliation boundary HSZ in southwestern AYD characterize the fold eastern limb and M–type foliation boundary discrete HSZ in the Poli region and YD characterize the fold respective hinges. The present–day overlap of the fold eastern and western limbs results from their relative displacement parallel to the CCSZ over 330 km, from position A to B. *Thin broken lines* outline axial plane HSZ. *Thick broken lines* outline F_3 fold profile. The grid delineates the map areas at 1/200.000. Other comments in the text.

The DSZ is of particular interest, as it shows a complex kinematic interaction with F_3 folds. Indeed, the finite strain pattern of the D_3 phase of deformation in both the low– to moderate–grade schists and the

high–grade granulitic gneisses enables to define two main structural domains (Figure 12): 1) the Demsa HSZ marked by anastomosing S–C–type foliation patterns, small– and large–scale pinch–and–swell structures generating symmetric and asymmetric boudins of metric to kilometric amphibolites and basic granulites competent layers, 2) the Poli fold zone marked by E–W–directed F_2 synforms and antiforms refolded by a large–scale F_3 asymmetric folds verging north. The F_3 overturned fold exhibits third or fourth–orders axial plane crenulation boundary cleavages. Its eastern reverse limb exhibits several third–order F_3 metric–scale recline folds verging to the south and plunging moderately to the west (Ngako, 1986). Its hinge zone verging to the north is characterized by fourth–order crenulation showing gradational boundaries. The mylonitization gradient in the DSZ is marked by discrete mylonitic HSZ in both the granulite gneisses and garnet–amphibolites that become thicker in the retrogressed gneisses marking their contact with the schists (Figure 12). The eastward plunges of the mineral lineations in the DSZ, as well as the geometry of the asymmetric profile of F_3 recline fold at the shear zone contact correlate with a down–slip relative displacement of the Poli Group.

3.4. HSZ Granitoids

The CAFB exhibits numerous meridian–directed shear zones generally agreed to control granitoids emplacements in WCD (Bella Nke et al., 2018; Fozing et al., 2021; Kwékam et al., 2020; Ngako et al., 2008; Nguiessi Tchankam et al., 1997; Njiki Chatué et al., 2020). Most of them represent map–scale analogues of S_3 axial plane crenulation boundary cleavages as exemplified in the present study by F_3 folds in the Ndikinimeki region (Figures 2, 9, and 10a). The migration of massive granitic melts through the HSZ and the late CCSZ channels and their ascent to the upper crustal levels during D_3 phase of deformation generated widespread granitoids intrusions (Figure 1).

Also note the strong analogy of the regional F_3 second–order folds and boundary HSZ geometry with the Borradaile–type small–scale patterns. Crustal slabs separated by successive HSZ are microlithons analogues. They represent WSZ and MSZ here defined as mesolithons or megalithons. (b) Second–order F_3 fold in the Tchamba HSZ reconstructed from Z–, S–, and M–type crenulation markers in the mesolithons remnants (outcrop TCH_6084; sheet 1, Figure 1). Intensely mylonitized mesolithons only show scarce remnants in the HSZ. However, M–type markers characterize F_3 second–order fold hinges, while Z– and S–types markers characterize F_3 second–order fold opposite limbs. S_3 cleavages mark the N160°E–directed HSZ and show steep–plunging mineral lineations. The progressive mylonitization of mesolithons parallel to S_3 cleavages results in the progressive widening of the HSZ up to metric and plurimetric widths (map view zonal–types). The latters are intruded by concordant and discordant more or less mylonitized granite massifs. Note the presence of random migmatites xenoliths more or less rotated in the late–D_3 cross–cutting intrusions.

Indeed, the high density of the N–S geophysical inferred HSZ network in the PRECASEM map area materializes discrete– or zonal–types S_3 first–order crenulation boundary cleavages analogues (Figure 9). This major conclusion shows that the spacing, density, and thickness of the crenulation boundary cleavages are scaled to the fold order and crenulation wavelengths. The longer the fold wavelength, the bigger the spacing of the boundary HSZ and the thicker the crenulation cleavages. Large–scale crenulation boundary cleavages in

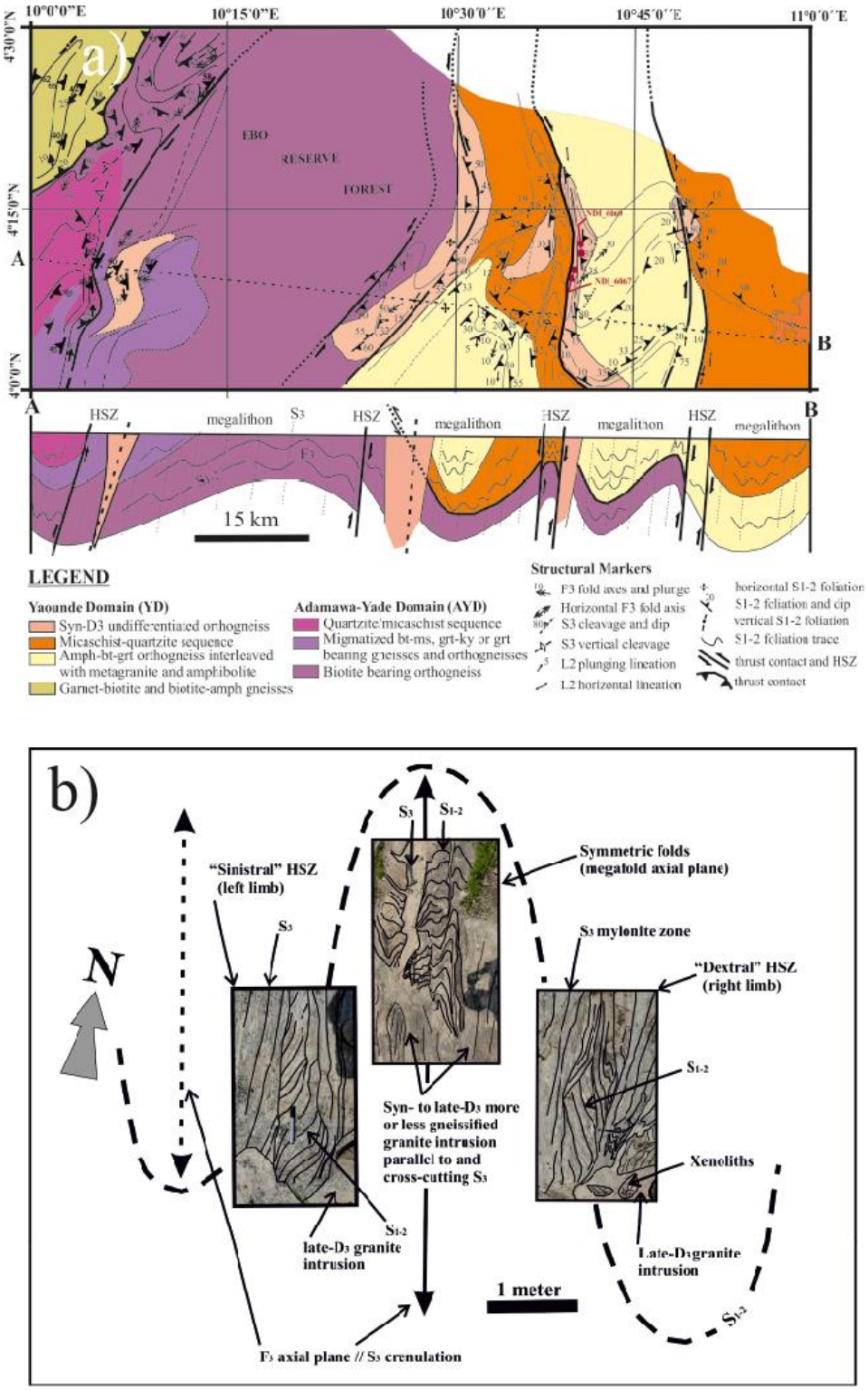

Figure 10. (a) Structure of the first–order F_3 fold hinge (see location in Figure 2) in the Ndikinimeki region. Second–order folds in megalithons show M–type crenulations and boundary HSZ. Note that S_{1-2} foliation trends exhibit similar F_3 folds geometry and transposition in both the YD and AYD.

CAFB represent weakened zones favorable to syn–D_3 granitoids emplacements (Figures 10b and 11). They show three main potential granitoids emplacements channels (Figure 2): 1) the N50°E–directed BNMB shear zones and related en echelon F_2 folds and nappes, which represent possible sites for diapiric intrusions, 2) the N30°E–directed axial plane boundary HSZ for the potential emplacements of early–D_3 granitoids, and 3) the N70°E–directed CCSZ and synthetics for potential emplacements of late–D_3 granitoids. Post–tectonic granitoids likely interacted with isostatic faults reactivation and crustal extension, as well as crustal erosion and detrital deposits in the Balche–type trenches. The magma source of the granitoids massifs during plate's convergence and collision is inferred to widespread partial melting at the base of the thickened crust during nappes stacking and/or to the ascent of the asthenosphere following crustal delamination during indentation processes (Ngako et al., 2008; Ngako & Njonfang, 2011, 2018). Indeed, in addition to nappes stacking and crustal thickening, the delamination of the lithospheric mantle during indentation is favorable to the ascent of hot asthenospheric material at the base of the crust, which generated large–scale partial melting in both the SFCC indent and ESB indenter. The anatectic melts inferred from these processes were channeled at different scales through crenulation boundary cleavages and HSZ to form granitoids intrusions in the upper crustal levels. Their emplacements were initiated as granitoid veins injections in the HSZ and S_3 crenulation boundary cleavages channels where increasing accumulation and ballooning of magmatic melts led to the emplacement of huge granitoid batholiths (Bella Nke et al., 2018; Njiki Chatué et al., 2020). The occurrences of small– and large–scale xenoliths of the wall rocks in those massifs probably result from hydraulic fragmentation of the crustal lithons during ballooning in magmatic chambers and forceful penetration of magma in the host rocks cleavages (Figures 10b and 11). Two main types of xenoliths occur in the CAFB massifs: xenoliths of the reactivated pieces of the SFCC deformed margin and xenoliths of the juvenile and supra–crustal metamorphic rocks.

4. Tectonic Implications: Discussion

4.1. Geotectonic Settings

The reconstruction of the CAFB geotectonic settings is a controversial topic, due to the relatively poor understanding of its complex structural evolution. Indeed, the imbalance developments of belt awareness in petrology, geochronology, geophysics, deformation, and structure permanently generate controversies about plates boundaries and nature (Abdelsalam et al., 2002; Affaton et al., 1991; Castaing et al., 1994; Fuh Calistus et al., 2021; Liégeois et al., 2013; Mvondo et al., 2023; Ngako, 2022; Ngako et al., 2008; Ngako & Njonfang, 2011, 2018; Penaye et al., 2006; Tchakounté Numben et al., 2018, 2021; Toteu et al., 2004, 2022; Trompette, 1994; etc.). We here provide global–scale strain assessments that shed more light on the configuration of the belt tectonic settings and evolution.

Indeed, the major geotectonic units in the CAFB are no more at their original positions. They were displaced over hundreds of kilometers, including basement slices of the colliding plates' margins within supra–crustal units, making correlations very difficult to assess. For instance, the AYD appears as flat–lying slices of the SFCC basement in the earlier nappe that was refolded, shifted away parallel to the CCSZ, and juxtaposed with different tectonic units. As well, the so–called northern and southern Cameroon were dextrally shifted parallel to the CCSZ and juxtaposed during D_3, after the upright folding episode of the related

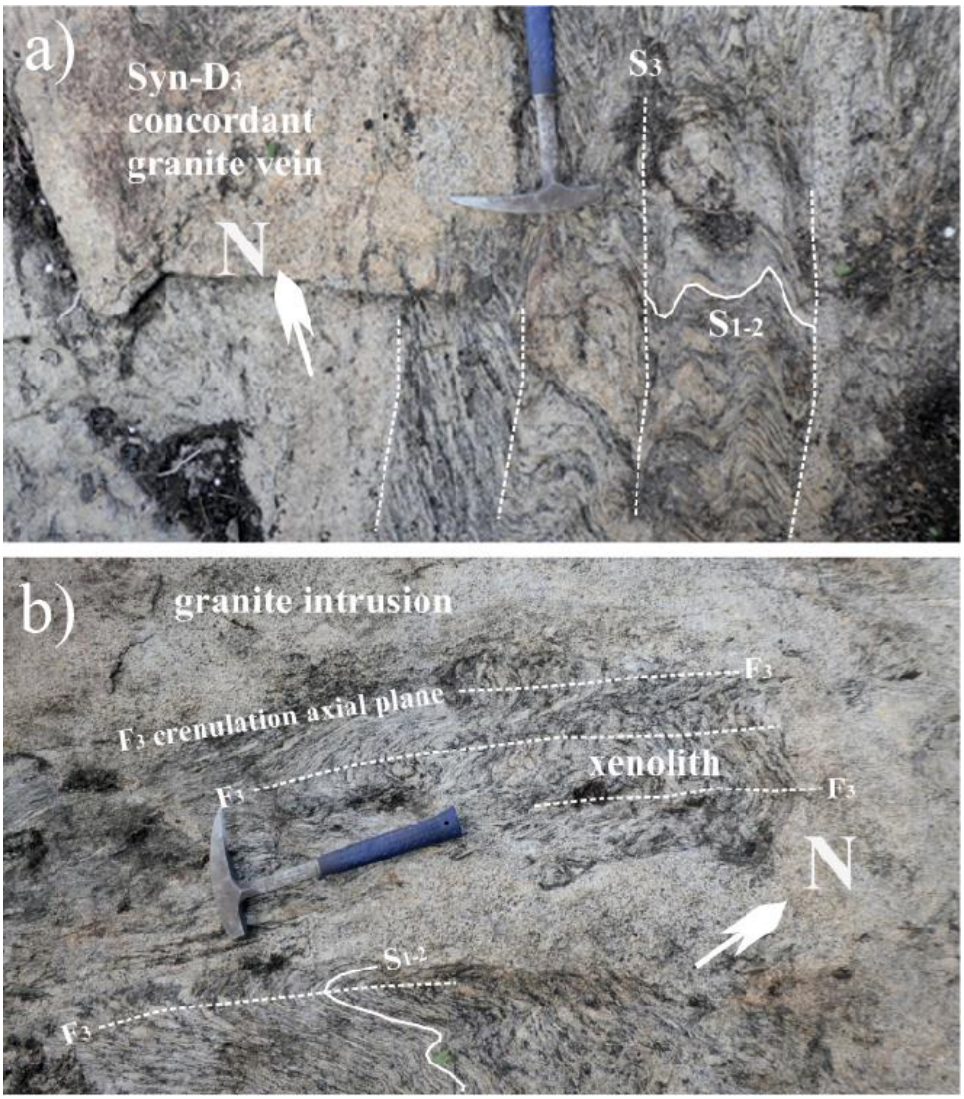

Figure 11. Structural interaction between HSZ and granitoid emplacements in migmatites (sheet 4, Figure 1. Outcrop BER_6058). (a) M–type crenulations and boundary HSZ directed N10°E showing gradational–, discrete–, and zonal–type patterns across N100°E–low–dipping $S_{1–2}$ foliation. Massive injections of anatectic melts in the crenulation boundary HSZ channels result in the emplacements of granite dykes and granite massifs; (b) Metric–size xenoliths in granitoid intrusion suggesting hydraulic fragmentation of the wall rock mesolithons. Horizontal YZ section. Hammer length is 30 cm.

units. The ideal unfolding of the F_3 first–order folds shows that the CAFB was only half its present width before the D_3 phase of deformation. As well, the restoration of $S_{1–2}$ foliation trends in their E–W original position prior to this deformation phase shows that the WCD, Poli Group, AYD, and YD originally represent lateral settings at the SFCC northern margins that were dextrally displaced along the CCSZ over more than a thousand kilometers. Other uncertainties concern the unknown amount of nappes relative displacements in the colliding plates' margins during the early $D_{1–2}$ tectonic evolution. Multiple relative displacements of tectonic units in thrust and wrench zones result in a very complex structural setting of the Pan–African belt that maintains controversial models of its tectonic history. Indeed, the tectonic

significance of geochronological data relies on accurate structural correlation of the dated tectonic units across the belt. For instance, the ages of syn–thrust granites in the earliest granulite nappes of Eastern–Nigeria at ca. 640 Ma (Ferré et al., 1998, 2002), concordant zircons in the VRSZ micaschists at ca. 630 Ma (Toteu et al., 1990), and pyriclasites in the Yaoundé nappes at ca. 620 Ma (Penaye et al., 1993) represent oldest post–collisional events approximated to the D_{1-2} phase in CAFB. They mark a diachronic post–collisional evolution inferred by some authors to serial microplate's collisions (Affaton et al., 1991; Penaye et al., 2006; Tchakounté Numbem et al., 2017; Toteu et al., 1987, 2022).

However, though the collision age in CAFB is still unknown, they could as well refer to different episodes of nappes stacking, as in the WAC margin where they occurred at 607, 587, and 579 Ma, respectively (Attoh et al., 1997), following continental collision precisely dated between 625 and 633 Ma (^{40}Ar–^{39}Ar ages of ultra–HP metamorphism on muscovite and phengite by Attoh et al. (1997) and Jahn et al., (2001)). A similar nappes stacking evolution upon the SFCC rigid margin during the collision with the ESC prong is also likely. Indeed, the global–strain geometry of the CAFB shows very strong similarities with the Himalayan one. In particular, the ESC prong intruded the SFCC indent, as the Indian indenter (passive margin) intruded the Eurasian indent (active margin) during the alpine orogeny. As in the Himalaya range, indentation of the SFCC margin generated several episodes of intraplate shear zones and nappes stacking in both the indenter and indent continents (Cobbold & Davy, 1988; Davy & Cobbold, 1988; Tapponnier et al., 1986). Similarly, major episodes of the early nappes staking in western Gondwana include: 1) NNE to NE–verging nappes onto the ESC passive margin between 680 and 640 Ma, inferred

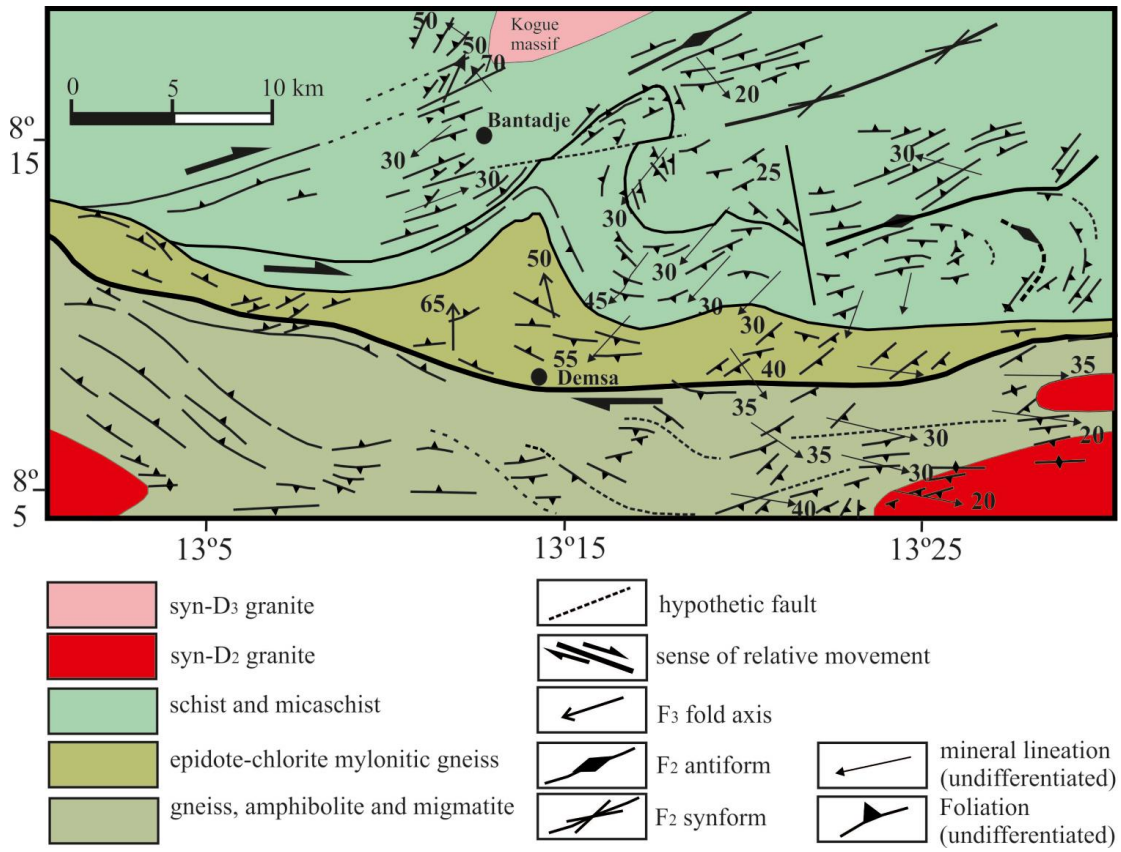

Figure 12. Structural map of the Demsa synthetic Shear Zone (DSZ).

to oblique collision of the western lateral boundary of the

The shear zone exhibits large–scale S–C–type pattern and boundary asymmetric F_3 fold profile in the Poli Group to the north. Large–scale boudins show pinch–and–swell patterns. The anastomosing geometry of S_3 and $S_{1–2}$ foliation trends, the F_3 fold asymmetric profile and vergence as well as the sense of mineral lineation plunges mark the down–slip displacement of the Poli Group to the east and its juxtaposition with the high–grade gneisses.

ESC prong with the Aouzegueur, Barghot, and Assode terranes following the N–S Raghane dextral shear zone (Liégeois et al., 1994; Ferre et al., 1998, 2002), 2) lateral expulsion nappes of the BNMB shear zone verging to the west at around 630 Ma at the prong frontal margin (Ngako et al., 2008; Toteu et al., 1990), and 3) southward verging nappes onto the SFCC at around 620 Ma (Penaye et al., 1993) inferred to the collision of the eastern concave margin of the prong with the SFCC active margin and the Sergipano–Yaoundé–Oubanguides supra–crust then situated to the east of the prong. As predicted by experimental models (Cobbold & Davy, 1988; Davy & Cobbold, 1988), the kinematics and chronology of these post–collisional nappes are related to the respective geometry of the prong and indent continent.

In CAFB, the detachment of the AYD block from the northern margin of the SFCC (Tchakounté Numbem et al., 2021) implies that the magmatic and sedimentary activities in the Yaoundé domain are coeval with the extension and breakup of this margin. However, considering the very narrow time gap between the oldest magmatic events in the YD dated at 666 Ma (Toteu et al., 2006), the closure of this basin at 625 Ma (Toteu et al., 2006), and the formation of the earliest post–collisional granulite nappes at 620 Ma (Penaye et al., 1993), it is more likely that these successive events are in continuity and in relation with a back–arc setting above a southward dipping subduction, as shown by the southward (Njonfang et al., 2006) and the westward (Liégeois et al., 1994) positive K–gradient in calc–alkaline orthogneisses in northern Cameroon and in Aïr. So far, no subduction–related ophiolites (Furnes and Dilek, 2017) have been reported in the Yaoundé basin, and the presence of MORB–like ophiolites therein (Mukete Kundu et al., 2022; Yonta Ngouné et al., 2010) only suggests that the back–arc extension evolved up to the oceanic stages. Nowadays, neither the crustal thickness map (Poudjom Djomani, 1993, Figure 1) nor the effective elastic thickness maps (Poudjom Djomani et al., 1995, Figure 13) suggest the presence of a microplate in the AYD. Rather, the direction of uplifted blocks and the relatively high crustal thinning in the AYD shows that this region is parallel to the belt root and axial zone where the nappes stacking and crustal thickening were maximum. Thus, it likely corresponds to the belt most elevated zone where the erosion rate and crustal thinning are also the highest. Indeed, plates and inferred rigid vestiges are supposed to be located at the belts margins, not within the belts roots or axial zones. This microplate model matches, neither with the above geophysical features, nor with the tectonic definition and concept of plates, which address rigid continents showing highly strained margins in collisional settings. Obviously, the AYD is made of reactivated pieces of the SFCC northern margin incorporated in supra–crustal units and strongly transposed, metamorphosed, and migmatized during the Pan–African tectonic evolution.

Thickness contour lines outline the finite position of the mantle plume interface with the belt uplifted root during isostatic stages, as well as the direction of the belt axial zone (see comments in the text).

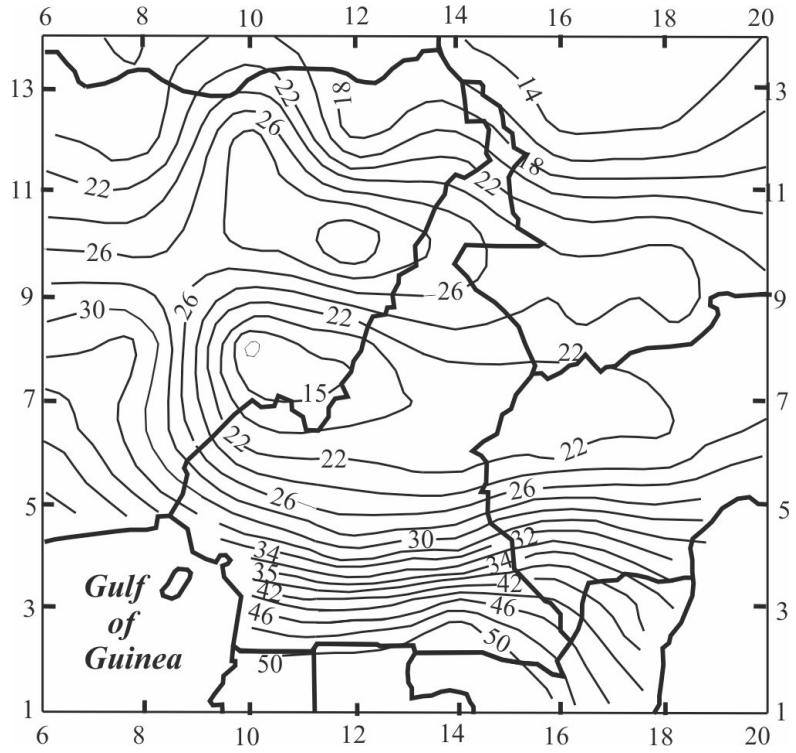

Figure 13. Crustal thickness map of the CAFB (in km) at the present erosion level in Cameroon and in the neighboring countries redrawn from Poudjom Djomani (1993).

Another important point for discussion relates to the nappes stacking processes upon the SFCC active margins. Indeed, orogenic belts classically show nappes stacking upon the passive margin. However, this rule is at variance in tectonic indentation settings (Cobbold & Davy, 1988; Davy & Cobbold, 1988; Tapponnier et al., 1986). Following the classical simple shear progressive models (Brun and Choukroune, 1981; Choukroune, 1995), the penetration of indenter into indent margin generates relative displacements at the crustal layers interfaces and the development of flat–lying mylonitic zones. These zones are interconnected by oblique mylonitic ramps enabling lower layers to override the upper ones. In the SFCC indent, the progressive mylonitization and rotation of the interconnecting ramps into parallelism with the layers interface shear planes likely ended with the formation of F_2 recumbent folds. The widespread occurrence of basic to intermediate calc–alkaline plutons in both the WCD, the Western Nigeria, and the AYD (Fitches et al., 1985; Toteu et al., 1987, 1990, 2001), the absence of significant effective elastic thickness records in these domains (Podjoum Djomani, 1993, Figure 1), and the rheological behavior of the SFCC blocks within the belt during the post–collisional evolution suggest that they represent basement vestiges of an archipelago–type cordillera tectonically reactivated and mixed–up with the WCD and YD supra–crustal units.

4.2. A Three-Plate Collision Model

A three–plate collision model offers the best explanation for the CAFB finite strain geometry. The nappes original trends reconstructed through the idealized unfolding of S_{1-2} foliation show that the WCD, Poli Group, AYD, and YD represent lateral geotectonic units bordering the northern margin of the SFCC (Figures 9 and 14). The foliation finite trends in

the post–collisional nappes materialize the global–scale overprint of upright folds (Figure 9). The regional structural interference correlates with two main shortening directions inferred to plate's convergences and terranes assembly in the N20°E and N120°E directions, in CAFB and Dahomeyan–Pharusian Fold belts, successively (Figure 14). Likely, the collision between the SFCC and ESC at unknown date and the progressive indentation of the SFCC margin by the ESC indenter generated several episodes of intra–belt nappes stacking at 680–640 (Ferré et al., 1998, 2002; Liégeois et al., 1994), 630 Ma (Ngako et al., 2008; Toteu et al., 1990), and 620 Ma (Penaye et al., 1993). Lately, the collision between the WAC and the SFCC deformed margin at ca 630–625 Ma (Attoh et al., 1997; Jahn et al., 2001) generated ultimate episodes of post–collisional nappes stacking upon the WAC at ca 607, 587, and 579 Ma (Attoh et al., 1997). We infer the meridian–directed trend in CAFB to the late overprinting of early D_{1-2} nappes by F_3 analogue folds following the collision of the SFCC deformed margin with the WAC. During this tectonic event, F_3 folds boundary HSZ behaved as channels for magma ascent and granitoids emplacements in the deforming crust between 600 and 580 Ma (Bella Nke et al., 2018; Fozing et al., 2021; Kwékam et al., 2020; Nguiessi Tchankam et al., 1997; Njiki Chatué et al., 2020). These ages fairly correlate with those of the post–collisional nappes stacking on the WAC, the dextral shear evolution in Central Cameroon and in Pernambuco, and the formation of respective meridian en echelon F_3 upright folds. The time gap between collision and nappes stacking in the Central African and the Dahomeyan–Pharusian fold belts shows that the edification of Western Gondwana mountain ranges in these tectonic settings

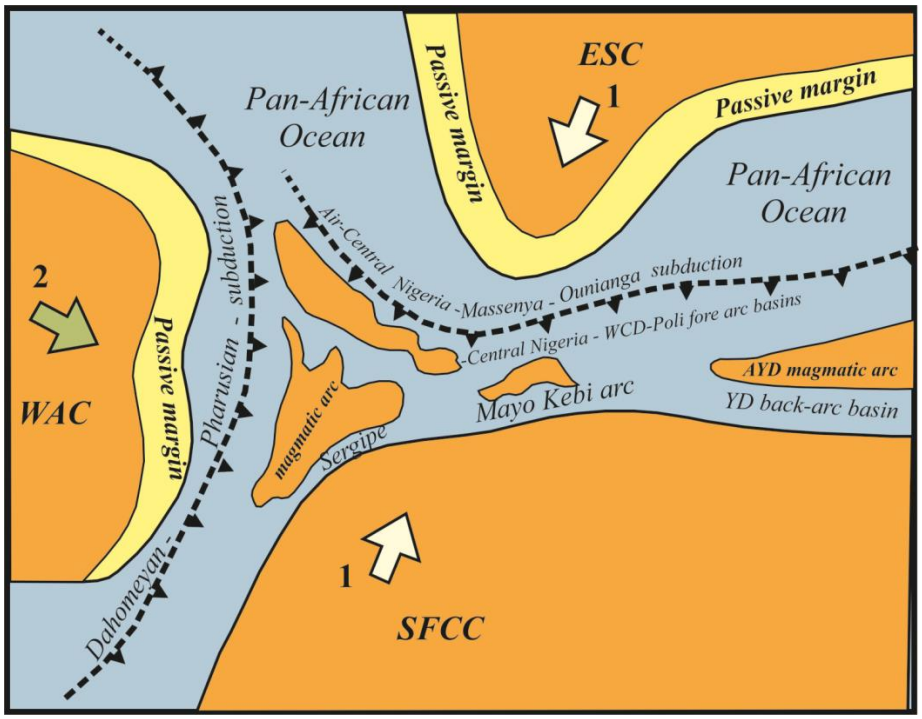

Figure 14. A three–plate convergence model in Western Gondwana during Neoproterozoic times. The AY blocks are interpreted as the vestiges of an archipelago–type cordillera overriding a southward–dipping subduction zone. 1 and 2 show the respective directions of plates' convergence and the inferred tectonic stresses during orogen 1 and orogen 2.

extended over 60 Myr and 20 Myr, respectively.

The change of tectonic stress directions in the CAFB is a global–scale feature that agrees with a three–plate collision model in Western Gondwana. In the NE Brazil central Borborema Province, the early top–to–south verging nappes and the en echelon meridian upright folds overprints oblique to the Pernambuco shear zone is inferred to a two–stage terranes assembly (de Lira Santos et al., 2017). In the Oubanguides (Central African Republic), this feature and origin were reported and questioned by Rolin (1995, 1992). However, as shown in Figure 9, the wavelengths of large–scale F_3 analogue folds seem to increase eastward and correlate with the progressive decrease of the strain intensity gradient during D_3, suggesting that F_3 fold amplitudes become weaker towards the Oubanguides domains where the early syn–D_{1-2} nappes are weakly refolded.

Acknowledgments

This work is a contribution of the PRECASEM mapping project at 1/200.000 of the Cameroon Ministry of Mines, Industry and Technological Development to the research on Gondwana History. We address our warmest thanks to the Cameroon government for the funding support. Additional thanks go to the two anonymous reviewers for their constructive comments and to editors for their careful work.

Data Availability Statement

The structural data are available in the Cameroon Web–site of the Cameroon Ministry of Mines, Industry and Technological Development, PRECASEM mapping Project (https://fr-sigm-online.hub.arcgis.com).

Authors contribution.

Ngako Vincent : Field works, data collection, data processing, paper conception, data interpretation, paper writing and editing.

Njonfang Emmanuel : Paper conception, data interpretation, paper editing.

Bernard Julien : Field works, data collection and data compilation.

Others : Field works and data collection.

References

Abdelsalam, M. G., Liégeois, J. P., & Stern, R. J. (2002). The Saharan metacraton. *Journal of African Earth Sciences, 34*, 119–136.

Affaton, P., Rahaman, M. A., Trompette, R., & Sougy, J. (1991). The Dahomeyide Orogen: Tectonothermal Evolution and relationships with the Volta Basin. *In* The West African 601, Orogens and Circum–Atlantic Correlatives, R. D. Dallmeyer and J. P. Lécorché (Eds), Springer–Verlag, 107–122.

Attoh, K., Dallmeyer, R. D., & Affaton, P. (1997). Chronology of nappes assembly in the Pan–African Dahomeyide orogen, West Africa: evidence from $^{40}Ar/^{39}Ar$ mineral ages. *Precambrian Research, 82*, 153–171.

Barbey, P., Macaudière, J., & Nzenti, J. P. (1990). High–pressure dehydration melting of metapelites: evidence from the migmatites of Yaoundé (Cameroon). *Journal of Petrology, 31*, 401–427.

Bayer, R., & Lesquer, A. (1978). Les anomalies gravimétriques de la bordure orientale du craton ouest africain : géométrie d'une suture panafricaine. *Bulletin Société Géologique de France, 7*, 863–876.

Bea, A., Cocheme, J. J., Trompette, R., Affaton, P., Soba, D., & Sougy, J. (1990). Grabens d'âge paléoprotérozoïque inférieur et volcanisme tholéïtique associé dans la région de Garoua, Nord–Cameroon. *Journal of African Earth Sciences, 10*, 657–667.

Bella Nke, B. E., Njanko, T., Mantani,

M. A., Njonfang, E., & Rochette, P. (2018). Kinematic evolution of the Mbakop Pan–African granitoids (Western Cameroon): an integrated AMS and EBSD approach. *Journal of Structural Geology, 111*, 42–63. https://doi.org/10.1016/j.jsg.2018.03.006

Black, R., Caby, R., Moussine–Pouchkine, A., Bayer, R., Bertrand, J. M., Boullier, A.M., et al. (1979). Evidence for late Precambrian plate tectonics in West Africa. *Nature, 278*, 223–226.

Borradaile, G. J., Bayly, M. B., & Powell, C. Mc. (1982). *Atlas of deformational and metamorphic rockfabrics*. Springer Verlag, Berlin, Germany, ISBN 3–540–11278–2 / 0–387–11278–2.

Bouyo Houketchang, M., Toteu, S. F., Deloule, E., Penaye, J., & Van Schmus, W. R. (2009). U–Pb and Sm–Nd dating of high–pressure granulite from Tcholliré and Banyo regions: evidence for a Pan–African granulite facies metamorphism in north–central Cameroon. *Journal of African Earth Sciences, 54*, 144–154. https://doi:10.1016/j.jafrearsci.2009.03.013

Brun, J. P., & Choukroune, P. (1981). Déformation progressive et structures crustales. *Revue de Géologie dynamique et de Géographie Physique, 23*, 177–193.

Burke, K. (2001). Origin of the Cameroon Line of volcano-capped swells. *Journal of Geology, 109*, 349–362.

Castaing, C., Feybesse, J. L., Thiéblemont, D., Triboulet, C., & Chèvremont, P. (1994). Palaeogeographical reconstructions of the Pan–African/Brasiliano orogen: closure of oceanic domain or intracontinental convergence between major blocks. *Precambrian Research, 69*, 327–344.

Choukroune, P. (1995). *Déformations et déplacements dans la croûte terrestre*. Masson, Paris, ISBN 2–225-84561–1.

Cobbold, P. R., & Davy, Ph. (1988). Indentation tectonics in nature and experiment. 2. Central Asia. *Bulletin of the Geological Institutions of Uppsala. N.S., 14*, 143–162. Uppsala. ISSN 0302–2749.

Davy, Ph., & Cobbold, P. R. (1988). Indentation tectonics in nature and experiment. 1. Experiment scaled for gravity. *Bulletin of the Geological Institutions of Uppsala. N.S., 14*, 129–141. Uppsala. ISSN 0302–2749.

De Lira Santos, Lauro Cé. M., Dantas, E. L., Vidotti, R. M., Cawood, P. A., dos Santos, E. J., et al. (2017). Two–stage terrane assembly in Western Gondwana: Insight from structural geology and geophysical data of central Borborema Province, NE Brazil. *Journal of Structural Geology*, *103*, 167–184 https://doi.org/10. 1016/j.jsg.2017.09.012.

Ferré, E. C., Caby, R., Peucat, J. J., Capdevilla, R., & Monié, P. (1998). Pan–African post–collisional ferro–potassic granite and quartz–monzonite plutons of Eastern Nigeria. *Lithos, 45*, 255–279.

Ferré, E. C., Gleizes, G., & Caby, R. (2002). Obliquely convergent tectonics and granite emplacement in the Trans–Saharan belts of Eastern Nigerian: a synthesis. *Precambrian Research, 114*, 199–219.

Fitches, W. R., Ajibade, A. C., Egbuniwe, I. G., Holt, R. W., & Wright, J. B. (1985). Late Proterozoic schist belts and plutonism in NW Nigeria. *Journal of Geological Society of London, 142*, 319–337.

Fozing, E. M., Kwékam, M., Tcheumenak Kouémo, J., Njanko, T., & Njonfang, E. (2021). Kinematic analysis of the Dschang granitic pluton (West–Cameroon): Implication to the Pan–African deformation of the Central African Fold Belt in Cameroon during the post–collisional history of western

Gondwana. *Precambrian Research, 359*. https://doi.org/10.1016/j.precamres.2021.106231

Fuh Calistus, G., Tchakounté Numbem, J., Mukete Kundu, O., Tchop, J. L., & Nkoumbou, C. (2021). Petrology, geochemistry, Ar–Ar isotopes of an arc related calc–alkaline pluton from Mamb (Pan–African Yaounde group, Cameroon): a testimony to the subduction of a hot oceanic crust. *Lithos, 384–385*. https://doi.org/10.1016/j.lithos.2021.105973

Furnes, H., & Dilek, Y. (2017). Geochemical characterization and petrogenesis of intermediate to silicic rocks in ophiolites: a global synthesis. *Earth Science Review, 166*, 1–37. http://dx.doi.org/10.1016/j.earscirev.2017.01.001

Ganwa, A. A. (2005). Les granitoïdes de Meiganga : étude pétrographique, géochimique, structurale et géochronologique. Leur place dans la chaîne panafricaine. Unpublished Doctorat d'Etat Thesis, University of Yaoundé I, Cameroon.

Jegouzo, P. (1984). *Evolution structurale du Sud-Ouest Cameroun durant l'orogène panafricain. Association de tectoniques cisaillante et chevauchante*. Colloque CNRS, chevauchement et déformation, Toulouse, p. 23.

Jahn, B., Caby, R., & Monie, P. (2001). The oldest UHP eclogites of the World: age of UHP metamorphism, nature of protoliths and tectonic implications. *Chemical Geology, 178*, 143–158.

Küster, D., & Liégeois, J. P. (2001). Sr–Nd isotopes and geochemistry of the Bayuda Desert high–grade metamorphic basement (Sudan): an early Pan–African oceanic convergent margin, not the edge of the East Saharan ghost craton? *Precambrian Research, 109*, 1–23.

Kwékam, M., Talla, V., Fozing, E. M., Tcheumenak kouémo, J., Dunkl, I., & Njonfang, E. (2020). The Pan–African high–K I–type granites from Batié complex, West Cameroon: age, origin and tectonic implications. *Frontiers in Earth Sciences, 8 (363)*, 1–14. https://doi: 10.3389/feart.2020.00363

Liégeois, J. P., Abdelsalam, M. G., Ennih, N., & Ouabadi, A. (2013). Metacraton: Nature, genesis and behavior. *Gondwana Research, 23*, 220–237. https://doi:10.1016/j.gr.2012.02.016

Liégeois, J. P., Black, R., Navez, J., & Latouche, L. (1994). Early and late Pan–African orogenies in the Aïr assembly of terranes (Tuareg shield, Niger). *Precambrian Research, 67*, 59–88.

Louis, P., 1970. Contribution géophysique à la connaissance du bassin du Lac Tchad. *Mémoire ORSTOM, Paris*.

Montes–Lauer, C. R., Trompette, R., Melfi, A. J., Bellieni, G., De Min, A., Bea, A., et al. (1997). *Pan–African Rb–Sr isochron of magmatic rocks from northern Cameroon. Preliminary results*. Paper presented at 9th South American Symposium on isotopic geology, Brazil.

Mvondo, H., Bineli Betsi, T., McFarlane C. R., Mvondo Ondoua, J. & Archibal, D. A. (2023). U–Pb and Ar–Ar geochronological constraints on timing of deformation and peak metamorphism in the Central Africa Orogenic Belt, Yaoundé Domain, Cameroon. *International Geology Review,* https://doi.org/10.1080/00206814.2023.2225183.

Mvondo, H., den Brok, S. W. J., & Mvondo Ondoa, J. (2003). Evidence for symmetric extension and exhumation of the Yaoundé nappe (Pan–African fold belt, Cameroon). *Journal of African Earth Sciences, 36*, 215–231.

Mukete Kundu, O., Minyem, D., Tamen, J, Nkoumbou, C., Fuh Calistus, G., & Tchakounté Numbem, J. (2022).

Petrology of ophiolites of Memel, Nsimè–Kellé and Mapan (Yaoundé group): evidence of the geodynamic evolution of the Pan–African orogeny in South Cameroon. *Journal of African Earth sciences, 191*, 1–24. https:// doi.org/10.1016/j.jafrearsci.2022.104357.

Nédélec, A., Macaudière, J., Nzenti, J. P., & Barbey, P. (1986). Evolution structurale et métamorphique des schistes de Mbalmayo (Cameroun). Implications pour la structure de la zone mobile panafricaine d'Afrique Centrale, au contact du craton du Congo. *Comptes Rendus de l'Académie des Sciences, Paris, 303*, 75–80

Nédélec, A., Myniem, D., & Barbey, P. (1993). High–P–high–T anatexis of Archaean tonalitic grey gneisses: the Eséka migmatites, Cameroon. *Precambrian Research, 62*, 191–205.

Ngako, V. (1986). Évolution métamorphique et structurale de la bordure sud–ouest de la série de Poli. Segment camerounais de la chaine panafricaine. *Mémoires et Documents du CAES n°5*, ISBN 2–905532–04–1.

Ngako, V. (1999). Les déformations continentales panafricaines en Afrique Centrale. Résultat d'un poinçonnement de type himalayen. Unpublished Doctorat d'Etat Thesis, University of Yaoundé I, Cameroon.

Ngako, V. (2022). *Géologie du Cameroun: Tectonique des plaques et évolution continentale de la formation à la destruction du Gondwana. Enjeux et défis de la recherche–développement*. Dorrance Edition, ISBN : 978-1-6480-4306-2, e-ISBN: 978-1-6480-4323-9.

Ngako, V., Affaton, P., & Njonfang, E. (2008). Pan–African tectonics in northwestern Cameroon: Implication for the history of western Gondwana. *Gondwana Research, 14*, 509–522. https:// doi:10.1016/j.gr.2008.02.002

Ngako, V., Affaton, P., Nnange, J. M., & Njanko, Th. (2003). Pan–African tectonic evolution in central and Southern Cameroon: transpression and transtension during sinistral shear movements. *Journal of African Earth Sciences, 36*, 207–214.

Ngako, V., Jégouzo, P., & Nzenti, J. P. (1991). Le Cisaillement Centre Camerounais. Rôle structural et géodynamique dans l'orogenèse panafricaine. *Comptes Rendus de l'Académie des Sciences, Paris, 313*, 457–463.

Ngako, V., & Njonfang, E. (2011). Plates amalgamation and Plate destruction. The Western Gondwana History. In Closson D. (ed.), *Tectonics, Intechopen*, ISBN 978–953–307–545–7, 3– 36.

Ngako, V., & Njonfang, E. (2018). Comment on « The Adamawa–Yade, a piece of Archean crust in the Neoproterozoic Central African Orogenic belt (Bafia area, Cameroon) » by Tchakounté et al. 2017. *Precambrian Research, 305*, 508–513. https://doi.org/10.1016/j.precamres.2017.12.004

Nguiessi Tchankam, C., Nzenti, J. P., Nkonguin Nsifa, E., Tempier, P., & Tchoua, F. (1997). Les granitoïdes calco–alcalins syn–cisaillement de Bandja dans la chaîne panafricaine nord–équatoriale au Cameroun. *Comptes Rendus de l'Académie des Sciences, Paris, 325*, 95–101.

Njel, U. O. (1986). Paléogéographie d'un segment de l'orogenèse panafricaine : la ceinture volcano– sédimentaire de Poli (Nord–Cameroun). *Comptes Rendus de l'Académie Sciences,Paris, 303*, 1737–1742.

Njiki Chatué, C., Njanko, T., Fozing, E. M., Bella Nke, B. E., Seta, N., & Njonfang, E. (2020). Field observations, magnetic fabrics and microstructures evidences of syn–kinematic emplacement of the Numba granite pluton (western Cameroon domain). *Journal of African Earth Sciences, 172*, 1–20. https://doi.

org/10.1016/j.jafrearsci.2020.104009

Njonfang, E., Ngako, V., Kwékam, M., & Affaton, P. (2006). The calc–alkaline orthogneiss of Foumban–Bankim: evidence of an inner sheared Pan–African active margin zone. *Comptes Rendus Géoscience, 338*, 606-616.

Nkoumbou, C., Yonta Ngouné, C., Villiéras, F., Njopwouo, D., Yvon, J., Ekodeck, G. E., & Tchoua, F. (2006). Découverte des roches à affinité ophiolitique dans la chaîne panafricaine au Cameroun : les talcschistes de Ngoung, Lamal Pougué et Bibodi Lamal. *Comptes Rendus Géoscience, 338*, 1167–1175.

Nzenti, J. P., Barbey, P., Macaudière, J., & Soba, D. (1988). Origin and evolution of the late Precambrian high–grade Yaoundé gneisses (Cameroon). *Precambrian Research, 38*, 91–754.

Penaye, J., Kröner, A., Toteu, S. F, Van Schmus, W. R., & Doumnang, J. C. (2006). Evolution of the Mayo Kebbi region as revealed by zircon dating: An early (c.a. 740 Ma) Pan–African magmatic arc in southwestern Chad. *Journal of African Earth Sciences, 44*, 530–542.

Penaye, J., Toteu, S. F., Van Schmus, W. R., & Nzenti, J. P. (1993). U–Pb and Sm–Nd preliminary geochronologic data on the Yaounde series, Cameroon: re–interpretation of the granulitic rocks as the suture of a collision in the "Centrafrican" belt. *Comptes Rendus de l'Académie des Sciences, Paris, 317*, 789–794.

Poudjom Djomani, Y. H. (1993). *Apport de la gravimétrie à l'étude de la lithosphère continentale et implications géodynamiques. Etude d'un bombement intraplaque : le massif de l'Adamaoua (Cameroun)*. Editions ORSTOM, Paris, France n° 109

Poudjom Djomani, Y. H., Nnange, J. M., Diament, M., Ebinger, C. J., & Fairhead, J. D. (1995). Effective elastic thickness and crustal thickness variations in west central Africa inferred from gravity data. *Journal of Geophysical Research, 100*, 22047–22070.

Ramsay, J. G., & Hubert, M. (1983). *The Techniques of Modern Structural Geology. Volume 1– Strain Analysis*. Academic Press, London.

Rolin, P. (1992). Présence d'un chevauchement ductile majeur d'âge panafricain dans la partie centrale de la République Centrafricaine : résultats préliminaires. *Comptes Rendus de l'Académie des Sciences, Paris*, 315, II, 467-470.

Rolin, P. (1995). La zone de décrochements panafricains des Oubanguides en République Centrafricaine. *Comptes Rendus de l'Académie des Sciences, Paris*, 320, IIa, 63-69.

Seme Mouangue, A. (1998). Géochimie, métamorphisme et métallogénie des formations ultrabasiques du secteur de Lomié (Sud–Est Cameroun). Unpublished Doctorat de 3ème cycle Thesis, University of Yaoundé I, Cameroon.

Soba, D., Michard, A., Toteu, S. F., Norman, D. I., Penaye, J., Ngako, V., et al. (1991). Données géochronologiques nouvelles (Rb–Sr, U–Pb et Sm–Nd) sur la zone mobile panafricaine de l'Est Cameroun : âge Protérozoïque Supérieur de la série du Lom. *Comptes Rendus de l'Académie des Science,s Paris, 312*, 1453–1458.

Tapponnier, P., Peltzer, G., & Armijo, R. (1986). On the mechanics of the collision between India and Asia. In MP Coward & AC Ries (eds.), *Collision Tectonics*, *Geological Society Special Publication,* 19, 115–157.

Tchakounté, J. (1999). Etude géologique de la région de Toundou–Bayomen dans la série de Bafia (Province du Centre). Tectonique, géochimie et métamorphisme. Unpublished Doctorat

3ème cycle Thesis, University of Yaoundé I, Cameroon.

Tchakounté Numbem, J., Eglinger, A., Toteu, S. F., Zeh, A., Nkoumbou, C., Mvondo Ondoua, J., et al. (2017). The Adamawa–Yade domain, a piece of Archean crust in the Neoproterozoic Central African Orogenic belt (Bafia area, Cameroon). *Precambrian Research, 299*, 210–229. http://dx.doi.org/10.1016/j.precamres.2017.07.001

Tchakounté Numbem, J., Fuh, C. G., Kamwa, A., Metang, V., Mvondo Ondoua, J., & Nkoumbou, C. (2021). Petrology and geochemistry of the Pan–African high–K calc–alkaline to shoshonitic–adakitic Bape plutonic suites (Adamawa–Yade block, Cameroon): evidence of a hot oceanic crust subduction. International Journal of Earth Sciences. https://doi.org/10.1007/s00531-021-02060-6.

Toteu, S. F. (1990). Geochemical characterization of the main petrographical and structural units of Northern Cameroon; implications for the Pan–African evolution. *Journal of African Earth Sciences, 10*, 615–624.

Toteu, S.F., Bertrand, J.M., Penaye, J., Macaudière, J., Angoua, S., & Barbey, P. (1991). Cameroon: a tectonic keystone in the Pan–African network. In: J.F. Lewry & M.R. Stauffer (Eds.), *The Early Proterozoic Trans–Hudson orogen of North America*, *Geological Association of Canada, Special Paper, 37*, 483–496.

Toteu, S.F., Macaudière, J., Bertrand, J.M., & Dautel, D. (1990). Metamorphic zircon from North Cameroon; implications for the Pan–African evolution of Central Africa. *Geologische Rundschau, 79*, 777–788.

Toteu, S. F., Michard, A., Bertrand, J. M., & Rocci, G. (1987). U–Pb dating of Precambrian rocks from northern Cameroon, orogenic evolution and chronology of the Pan–African belt of central Africa. *Precambrian Research, 37*, 71–87.

Toteu, S. F., Penaye, J., Deloule, E., Van Schmus, W. R., & Tchameni, R. (2006). Diachronous evolution of volcano–sedimentary basins north of the Congo craton: Insights from U–Pb ion microprobe dating of zircons from the Poli, Lom and Yaounde Groups (Cameroon). *Journal of African Earth Sciences, 44*, 428–442.

Toteu, S. F., Penaye, J., & Poudjom Djomani, Y. H. (2004). Geodynamic evolution of the Pan–African belt in Central Africa with special reference to Cameroon. *Canadian Journal of Earth Sciences, 41*, 73–85.

Toteu, S. F., Van Schmus, W. R., Penaye, J., & Nyobé, J. B. (1994). U–Pb and Sm–Nd evidence for Eburnean and Pan–African high–grade metamorphism in cratonic rocks of Southern Cameroon. *Precambrian Research, 67*, 321–347.

Toteu, S. F., Van Schmus, Penaye, J., & Michard, A. (2001). New U–Pb and Sm–Nd data from North– Central Cameroon and its bearing on the pre–Pan–African history of Central Africa. *Precambrian Research, 108*, 45–73.

Toteu, S. F., Wit, M., Penaye, J., Drost, K., Tait, J. A., Houketchang Bouyo, M., et al. (2022). Geochronology and correlations in the Central African Fold Belt along the northern edge of the Congo Craton: New insights from U–Pb dating of zircons from Cameroon, Central African Republic, and south–western Chad. *Gondwana Research, 107*, 296–324. https://doi.org/10.1016/j.gr.2022.03.010

Trompette, R. (1994). *Geology of Western Gondwana (2000–500 Ma). Pan–African–Brasiliano aggregation of South America and Africa*. Balkema, A.A.: Rotterdam.

Yongue Fouateu, R. (1995). Les

concentrations métallifères de nickel et de cobalt à partir de l'altération latéritique des roches ultrabasiques serpentinisées du Sud–Est Cameroun. Unpublished Doctorat d'Etat thesis, University of Yaoundé I, Cameroon

Yonta Ngouné, Cl., Nkoumbou, C., Barbey, P., Le Breton, N., Montel, J. Mc, & Villette, P. (2010). Geological context of the Boumyebel talcschists (Cameroon): inferences on the Pan–African belt of Central Africa. *Comptes Rendus Géoscience, Paris, 342*, 108–115